



2017

Enhanced Potency of Bivalent Small Molecule gp41 Inhibitors

Vladimir Sofiyev

Hardeep Kaur

Touro University California, hardeep.kaur@tu.edu

Beth A. Snyder

Priscilla A. Hogan

Roger G. Ptak

See next page for additional authors

Follow this and additional works at: https://touro scholar.touro.edu/tucom_pubs



Part of the [Amino Acids, Peptides, and Proteins Commons](#), and the [Immune System Diseases Commons](#)

Recommended Citation

Sofiyev, V., Kaur, H., Snyder, B. A., Hogan, P. A., Ptak, R. G., Hwang, P., & Gochin, M. (2017). Enhanced potency of bivalent small molecule gp41 inhibitors, *Bioorganic & Medicinal Chemistry*, 25(1), 408-420.

Authors

Vladimir Sofiyev, Hardeep Kaur, Beth A. Snyder, Priscilla A. Hogan, Roger G. Ptak, Peter Hwang, and Miriam Gochin

Accepted Manuscript

Enhanced potency of bivalent small molecule gp41 inhibitors

Vladimir Sofiyev, Hardeep Kaur, Beth A. Snyder, Priscilla A. Hogan, Roger G. Ptak, Peter Hwang, Miriam Gochin

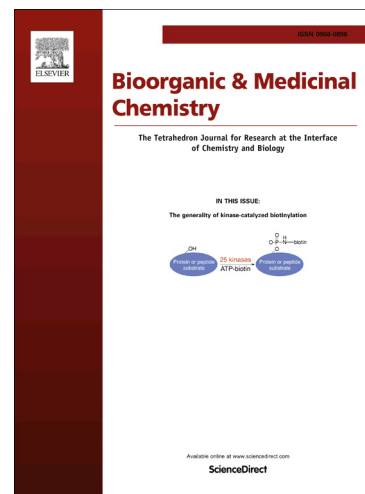
PII: S0968-0896(16)30774-X
DOI: <http://dx.doi.org/10.1016/j.bmc.2016.11.010>
Reference: BMC 13377

To appear in: *Bioorganic & Medicinal Chemistry*

Received Date: 20 September 2016
Revised Date: 31 October 2016
Accepted Date: 3 November 2016

Please cite this article as: Sofiyev, V., Kaur, H., Snyder, B.A., Hogan, P.A., Ptak, R.G., Hwang, P., Gochin, M., Enhanced potency of bivalent small molecule gp41 inhibitors, *Bioorganic & Medicinal Chemistry* (2016), doi: <http://dx.doi.org/10.1016/j.bmc.2016.11.010>

This is a PDF file of an unedited manuscript that has been accepted for publication. As a service to our customers we are providing this early version of the manuscript. The manuscript will undergo copyediting, typesetting, and review of the resulting proof before it is published in its final form. Please note that during the production process errors may be discovered which could affect the content, and all legal disclaimers that apply to the journal pertain.



© 2016. This manuscript version is made available under the CC-BY-NC-ND 4.0 license <http://creativecommons.org/licenses/by-nc-nd/4.0/>

Enhanced potency of bivalent small molecule gp41 inhibitors

Vladimir Sofiyev^a, Hardeep Kaur^a, Beth A. Snyder^c, Priscilla A. Hogan^c, Roger G. Ptak^c, Peter Hwang^d and Miriam Gochin^{a,b*}

^a *Department of Basic Sciences, Touro University-California, Vallejo, CA 94592*

^b *Department of Pharmaceutical Chemistry, University of California San Francisco, CA 94143*

^c *Southern Research Institute, 431 Aviation Way, Frederick, Maryland 21701*

^d *Department of Biophysics and Biochemistry, University of California San Francisco, CA 94143*

* M. Gochin: Touro University - California, 1310 Club Drive, Mare Island, Vallejo, CA 94592.

Tel. (707) 638-5463; FAX: (707) 638-5255; e-mail: miriam.gochin@tu.edu

Abstract

Low molecular weight peptidomimetic inhibitors with hydrophobic pocket binding properties and moderate fusion inhibitory activity against HIV-1 gp41-mediated cell fusion were elaborated by increasing the available surface area for interacting with the heptad repeat-1 (HR1) coiled coil on gp41. Two types of modifications were tested: 1) increasing the overall hydrophobicity of the molecules with an extension that could interact in the HR1 groove, and 2) forming symmetrical dimers with two peptidomimetic motifs that could potentially interact simultaneously in two hydrophobic pockets on the HR1 trimer. The latter approach was more successful, yielding 40 – 60 times improved potency against HIV fusion over the monomers. Biophysical characterization, including equilibrium binding studies by fluorescence and kinetic analysis by Surface Plasmon Resonance, revealed that inhibitor potency was better correlated to off-rates than to binding affinity. Binding and kinetic data could be fit to a model of bidentate interaction of dimers with the HR1 trimer as an explanation for the slow off-rate, albeit with minimal cooperativity due to the highly flexible ligand structures. The strong cooperativity observed in fusion inhibitory activity of the dimers implied accentuated potency due to the transient nature of the targeted intermediate. Optimization of monomer, dimer or higher order structures has the potential to lead to highly potent non-peptide fusion inhibitors by targeting multiple hydrophobic pockets.

Keywords: HIV-1 gp41; hydrophobic pocket; fusion inhibition; peptidomimetic inhibitors, bivalent inhibitors; fluorescence; surface plasmon resonance; kinetics; cooperativity.

1. Introduction

The hydrophobic pocket (HP) on the surface of the gp41 trimeric HR1 coiled coil is an important target for antiretroviral drugs against HIV fusion.¹ The pocket sits at the interface between HR1 and helical HR2 segments which wrap down the sides of the coiled coil to form a six-helix bundle structure upon successful virus – host membrane fusion (Figure 1A).^{2,3} The pocket is exposed to inhibitors for 20 – 30 minutes during a conformational change of gp41 prior to six-helix bundle formation.⁴ Small molecules that bind in this pocket have been developed into low to sub- μM inhibitors of HIV entry,⁵⁻⁸ but so far efforts at small molecule discovery have failed to achieve the potency afforded by C-peptides derived from HR2.^{9,10} These are nM inhibitors, including T20 which is an FDA-approved fusion inhibitor.¹¹ Non-peptide inhibitors of HIV fusion could have advantageous properties as drugs, such as longer half-life and lower cost and the potential for oral bioavailability.

One approach to improving potency of small molecules is to extend them to form additional interactions with HR1 beyond the hydrophobic pocket. HR1 has multiple potential interactive sites both within a single groove and between adjacent grooves of the trimer. Bidentate ligands are generally 1 – 2 orders of magnitude more potent than their monomeric counterparts against targets with more than one binding site.^{12,13} To our knowledge, this concept has not been tested with small molecule inhibitors targeting gp41. For C-peptides, the effect of multivalent interactions is clear. 18 residue HP-binding C-peptides containing the motif WxxWDxxI are low μM binders^{14,15} and fusion inhibitors,¹⁶ while 34 residue C-peptides have low nM activity.¹⁷ Dimerization of 22 residue helical C-peptides improved activity by a factor of 9.¹⁸ Similarly, D-peptides designed to bind in the hydrophobic pocket¹⁹ have activity improved

by 10 – 300 fold upon dimerization with a long polyethylene glycol (PEG) linker, presumably by simultaneous interactions in two HP's of the trimer.^{20, 21}

An important consideration in designing extension or dimerization of small molecule hydrophobic pocket binders is selection of a tether that will not disturb the binding mode. Helical peptidomimetics are suitable candidates for this approach because they are designed to emulate the amphipathic C-peptide helix, which has HP binding residues on one face of the helix (Fig 1B).

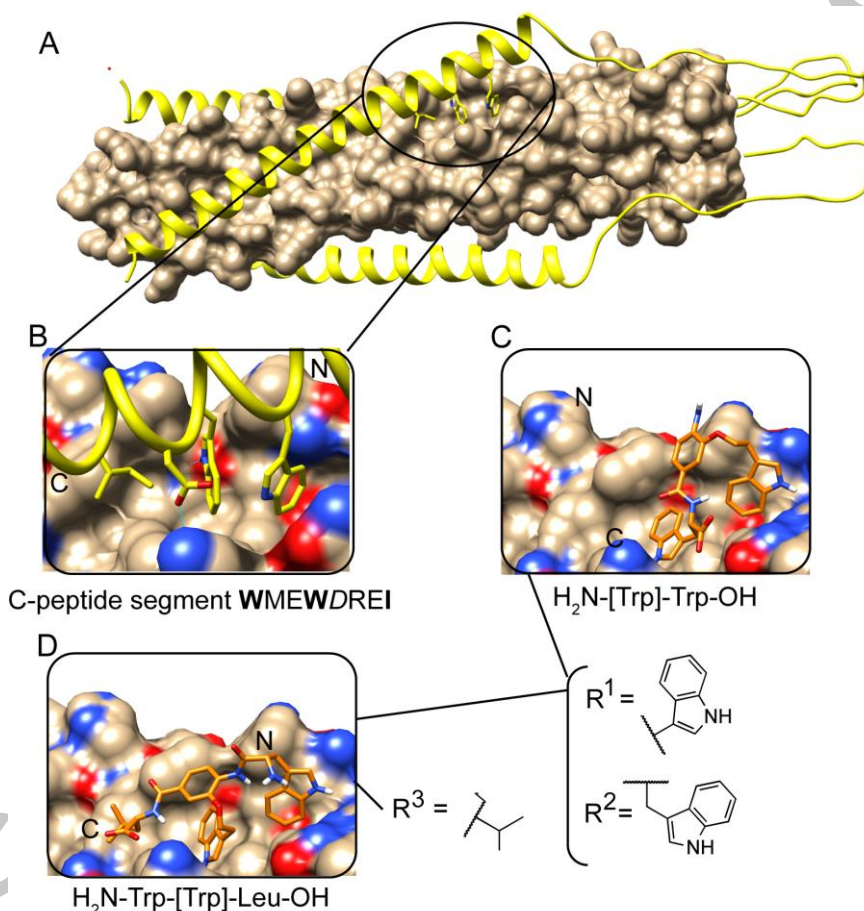


Figure 1. Experimental and model structures of the gp41 HR1 – HR2 domain and interactions. A. Homology modeling of HIV-1 HXB2 ectodomain from the structure of the corresponding SIV domain (pdb 2EZO). The HR1 trimer is shown as a space filling model in tan, and loop and HR2 residues are shown as a ribbon representation in yellow; B. Expansion of the hydrophobic pocket region from A. C, D. Modeled low energy structures of two subunit and three subunit peptidomimetics with Trp and Leu residues filling the pocket. See Figure 2 for the structures of the peptidomimetic inhibitors.

Peptidomimetic inhibitors are expected to have side chains occupying the pocket while the non-peptidic “backbone” is exposed above the pocket and available for tethering.

We previously examined a combinatorial library of three-subunit peptidomimetics containing a central aryl-alkoxy scaffold replacing the peptide backbone, $H_2N-R^3-[R^2]-R^1-OH$, as well as the precursor two-subunit library, $O_2N-[R^2]-R^1-OH$, developed by the Boger group.²² Screening with a binding assay for the gp41 hydrophobic pocket revealed a clear propensity for aromatic residues at R^1 and R^2 , especially for Trp, Nap and Phe4Cl.²³ Ile was also well-tolerated at R^1 in three subunit compounds with an aryl R^3 , consistent with the inhibitors emulating the conserved WWI motif of gp41 C-peptides. The compounds $H_2N-Asn-[Trp]-Trp-COOH$ ($K_I = 0.8 \mu M$, $IC_{50}^{CCF} = 6 \mu M$) and $H_2N-Trp-[Trp]-Leu-COOH$ ($K_I = 1.3 \mu M$, $IC_{50}^{CCF} = 5 \mu M$) were among the most potent compounds. In the absence of R^3 in the two subunit compounds, $R^2 = Trp$ or Nap and $R^1 = Trp$, Nap or Phe4Cl were the optimal choices. Bioactivity was reduced by a factor of ~4 compared to the three subunit compounds listed.²⁴

Most low energy simulated structures adopted the predicted binding pose in which the side chains reached down into the pocket and the aryl alkoxy “backbone” lay above the pocket (Figure 1C, D). NMR paramagnetic relaxation enhancement measurements on two inhibitors of this class, $O_2N-[HoPhe]-Ala-OH$ and $O_2N-[Ala]-Nap-OH$ confirmed this binding mode.²⁴ We selected two subunit compounds with $R^1 = Trp$ or Phe4Cl and $R^2 = Trp$ to explore attachment of a tether to the aryl alkoxy moiety, and to evaluate the effect of extension or dimerization on binding affinity and inhibition of virus – cell and cell – cell fusion.

2. Materials and Methods

2.1 Synthetic chemistry

2.1.1. Sources 3-fluoro-4-nitrobenzoic acid was purchased from Matrix Scientific (Fisher), 3-(2-hydroxyethyl)indole, Zn nanopowder, was purchased from Sigma-Aldrich. THF was purchased from EMD Millipore (VWR). 4-chlorobenzylalcohol was purchased from Alfa Aesar. L-tryptophan tert-butyl ester hydrochloride was purchased from Chem-Impex International.

2.1.2 Preparation of the aryl subunits The aryl subunits were synthesized following the general procedure described previously.²²

1. $R^2 = 3$ -ethyleneindole. Sodium hydride (60%, 0.5 g, 12.5 mmol) and 3-(2-hydroxyethyl)indole (1.0 g, 5.4 mmol) were stirred in 10ml THF at 0°C for 15 minutes, after which 3-fluoro-4-nitrobenzoic acid (1.04 g, 6.45 mmol) was added. The mixture was stirred at 0°C overnight, and then quenched with aqueous saturated NH_4Cl , diluted with ethyl acetate, washed with 0.1M HCl (50ml, x 2). The organic layer was concentrated and purified by silica gel chromatography (10:1 DCM/ MeOH, 1% acetic acid) , affording 2.6 g pure product (74%). Data for **1**: ^1H NMR (DMSO) δ 7.87 (d, 1H, J = 8.4 Hz), 7.81 (s, 1H), 7.62 (dd, 1H, J = 8.3 Hz, 0.8 Hz), 7.58 (d, 1H, J = 7.8 Hz), 7.36 (d, 1H, J = 8.0 Hz), 7.23 (d, 1H, J = 1.9 Hz), 7.07 (t, 1H, J = 7.3 Hz), 6.98 (t, 1H, J = 7.4 Hz), 4.43 (t, 2H, J = 6.9 Hz), 3.18 (t, 2H, J = 6.9 Hz).

2. $R^2 = 4$ -chlorobenzyl. Sodium hydride (60%, 0.68 g, 17 mmol) and 4-chlorobenzylalcohol (1.21 g, 8.5 mmol) were stirred in 15ml THF at 0°C for 15 minutes, after which 3-fluoro-4-nitrobenzoic acid (1.5 g, 8.1 mmol) was added. The mixture was stirred at 0°C overnight, and then quenched with aqueous saturated NH_4Cl , diluted with ethyl acetate, washed with 0.1M HCl (75ml, x 2) and brine. The organic layer was concentrated and separated by silica gel chromatography (3:2:0.1 hexanes/ ether/acetic acid \rightarrow 10 : 1 DCM/MeOH) to yield 2.2 g product **5** (89%). Data for **2**: ^1H NMR (DMSO) δ 8.00 (d, 1H, J = 8.3 Hz), 7.86 (d, 1H, J = 1.4 Hz), 7.67 (dd, 1H, J = 8.3 Hz, 1.5 Hz), 7.49 (s, 4H), 5.39 (s, 2H).

2.1.3 Preparation of 2-unit peptidomimetics followed procedures similar to those described previously.²²

3a. (O-tBu) Compound **1** (605 mg, 1.85 mmol) and L-Trp t-butyl ester (550 mg, 1.85 mmol) were combined in 12ml dry DMF to which EDCI (426 mg, 2.22 mmol), HOBt (300mg, 2.22 mmol) and DIPEA (0.97 ml, 5.57 mmol) were added. The solution was stirred overnight, then diluted with EtOAc, washed with sodium bicarbonate, 10% NaCl (x2), brine, and then concentrated. 850 mg of product was obtained on a flash column in 40% EtOAc /hexane, $R_f = 0.35$ and used immediately for the next reaction. The product (850 mg, 1.49 mmol) was reduced by dissolving it in 24 ml of 5:1 acetone : water and adding Zn nanopowder (978 mg, 15.0 mmol), and NH_4Cl (1.2 g, 22.4 mmol). An instantaneous exothermic reaction occurred, after which the mixture was filtered, diluted with 1 : 1 EtOAc/ether, washed with bicarbonate and brine and evaporated. The solid was triturated and purified by silica gel chromatography (50% EtOAc/hexane) to afford **3** in quantitative yield. Data for **3a**: $R_f = 0.30$ (50% EtOAc/hexane); MS calc. 538.64, found $(\text{M-H})^-$ 537.12; $^1\text{H NMR}$ (CDCl_3) δ 8.16 (br, 1H), 8.05 (br, 1H), 7.65 (d, 1H, $J = 7.9$ Hz), 7.60 (d, 1H, $J = 7.9$ Hz), 7.36 (d, 1H, $J = 8.0$ Hz), 7.25 (m, 1H), 7.20 (m, 2H), 7.16 – 6.99 (m, 6H), 6.54 (d, 1H, $J = 8.1$ Hz), 6.50 (d, br, 1H, $J = 7.52$), 5.02 (m, 1H), 4.19 (t, 2H, $J = 6.7$ Hz), 3.37 (m, 2H), 3.22 (t, 2H, $J = 6.7$ Hz), 1.40 (s, 9H).

3. Ester **3a** (213 mg, 0.396 mmol) was taken up in dry HCl in dioxane (4 M, 6.0 mL), stirred for 1.5 h, and concentrated. Purification by silica gel chromatography (1:4 MeOH:DCM) and filtration through a plug of Celite using acetone as the solvent yielded carboxylic acid **3** (180 mg, 94%). Data for **3**: MS calculated 482.53, found $(\text{M-H})^-$ 481.30; $^1\text{H NMR}$ (acetone) δ 7.68 (m, 2H), 7.41 – 7.25 (m, 6H), 7.13 – 6.96 (m, 4H), 6.65 (d, 1H, $J = 7.7$ Hz), 5.00 (m, 1H), 4.19 (t, 2H, $J = 6.6$ Hz), 3.47 – 3.35 (m, 2H), 3.24 (t, 2H, $J = 6.6$ Hz).

4a. (O-tBu) Compound **4** was prepared from compound **2** using the same method as for preparation of compound **3**. Purification by silica gel chromatography (40% EtOAc/hexane) yielded **4** (781 mg, 92%). Data for **4**: $R_f = 0.18$ (40% EtOAc/ hexane); $^1\text{H NMR}$ (CDCl_3) δ 9.14 (br, 1H), 8.32 (d, 1H, $J = 8.4$ Hz), 7.94 (s, 1H), 7.58 (d, 1H, $J = 7.9$ Hz), 7.30 – 7.24 (m, 6H), 7.13 – 7.07 (m, 2H), 7.02 (m, 2H), 6.92 (d, 1H, $J = 7.4$ Hz), 4.97 (q, 1H, $J = 7.0$ Hz), 4.81 (br, 2H), 3.36 (m, 4H)

4. Ester **4a** (168 mg, 0.324 mmol) was taken up in dry HCl in dioxane (4 M, 3.0 mL), stirred for 1 h, and concentrated. Purification by silica gel chromatography (1:9 MeOH:DCM) yielded carboxylic acid **4** (93.2 mg, 62%). Data for **4**: MS Calc. 463.91, found (M-H) $^-$ 462.17; $^1\text{H NMR}$ (acetone) δ 7.68 (d, 1H, $J = 7.8$ Hz), 7.48 – 7.36 (m, 6H), 7.30 – 7.28 (m, 2H), 7.08 (t, 1H, $J = 7.7$ Hz), 7.01 (t, 1H, 7.4 Hz), 6.68 (d, 1H, $J = 8.0$ Hz), 5.04 (s, 2H), 5.00 (br, ~1H), 3.5-3.4 (m, 2H).

2.1.4 Preparation of bivalent compounds

5. Solution of amine **3a** (543 mg, 1.01 mmol) and succinic anhydride (134 mg, 1.33 mmol) in THF (10 mL) was stirred for 4 h at 65°C. Purification by silica gel chromatography (7:3 EtOAc/hexane) afforded **5** (637 mg, 99%). Data for **5**: $R_f = 0.40$ (10:1 DCM:MeOH). $^1\text{H NMR}$ (CDCl_3) δ 8.75 (s, 1H), 8.65 (s, 1H), 8.16 (d, 1H, $J = 8.2$ Hz), 7.72 (s, 1H), 7.57 (d, 1H, $J = 7.9$ Hz), 7.53 (d, 1H, $J = 7.3$ Hz), 7.28 – 7.22 (m, 3H), 7.12 – 6.99 (m, 5H), 6.96 (d, 1H, $J = 1.8$ Hz), 6.89 (d, 1H, $J = 7.6$ Hz), 6.84 (d, 1H, $J = 1.7$ Hz), 5.00 (q, 1H, $J = 7.4$ Hz, 5.8 Hz), 3.99 (t, 2H, $J = 5.5$ Hz), 3.44 – 3.29 (m, 2H), 3.02 (t, 2H, $J = 5.5$ Hz), 2.54 (t, 2H, $J = 6.1$ Hz), 2.20 (t, 2H, $J = 5.8$ Hz), 1.42 (s, 9H).

6. Solution of amine **4a** (456 mg, 0.88 mmol) and succinic anhydride (111 mg, 1.10 mmol) in THF (8 mL) was stirred overnight at 54°C. Purification by silica gel chromatography (4:1

EtOAc/hexane \rightarrow EtOAc) afforded **6** (306 mg, 56%). Data for **6**: $^1\text{H NMR}$ (CDCl_3) δ 8.86 (s, 1H), 8.21 (d, 1H, $J = 8.2$ Hz), 8.08 (s, 1H), 7.57 (d, 1H, $J = 7.7$ Hz), 7.30 – 7.27 (m, 4H); 7.22 – 7.20 (m, 2H), 7.11 – 7.07 (m, 2H), 7.04 – 7.00 (m, 2H), 6.95 (d, 1H, $J = 7.6$ Hz), 4.98 (q, 1H, $J = 7.3$ Hz, 5.7 Hz), 4.82 (s, 2H), 3.42 – 3.29 (m, 2H), 2.69 – 2.58 (m, $>4\text{H}$), 1.41 (s, 9H).

7 Solution of triethylene glycol diamine ($\text{H}_2\text{N}-(\text{CH}_2\text{CH}_2\text{O})_3-\text{CH}_2\text{CH}_2\text{NH}_2$) (24.6 mg, 0.128 mmol), carboxylic acid **5** (130. mg, 0.204 mmol), EDCl.HCl (54.0 mg, 0.282 mmol), HOAt (37.2 mg, 0.273 mmol) and DIPEA (0.11 mL, 0.63 mmol) in DMF (2.0 mL) was stirred for 18 h. Purification by silica gel chromatography (10:1 DCM:MeOH) afforded the intermediate *t*Bu ester-protected dimer (143 mg). Data for *t*Bu ester-protected dimer: $^1\text{H NMR}$ (CDCl_3) δ 9.32 (s, br, 1H), 8.95 (s, br, 1H), 8.13 (d, 1H, $J = 8.5$ Hz), 7.99 (s, 1H), 7.86 (s, 1H), 7.55 (m, 2H), 7.32 (d, 1H, $J = 7.9$ Hz), 7.26 (d, 1H, $J = 8.5$ Hz), 7.22 (s, br, 1H), 7.08 (m, 3H), 7.00 (m, 2H), 6.95 (d, 1H, $J = 1.9$ Hz), 6.91 (d, 1H, $J = 7.5$ Hz), 6.86 (t, 1H, $J = 5.1$ Hz), 4.98 (q, 1H, $J = 7.0$ Hz), 4.01 (t, 2H, $J = 5.9$ Hz), 3.52 (br, 4H), 3.46 (t, 2H, $J = 4.6$ Hz), 3.38 (m, 4H), 3.06 (t, 2H, $J = 5.4$ Hz), 2.36 (m, 4H), 1.41 (s, 9H).

This intermediate (143 mg) was taken up in dry HCl in dioxane (4 M, 2.0 mL), stirred for 70 min, and concentrated under a stream of Ar. Purification by silica gel chromatography (10:1 DCM:MeOH \rightarrow 4:1 [90:10:0.6:0.6 CH_2Cl_2 :MeOH:H₂O:NH₄OH]:MeOH) afforded dimer **7** (55.4 mg, 41% over 2 steps). Data for **7**: $R_f = 0.20$ (10:1 DCM:MeOH); MS calculated: 1335.43 (ammonium salt), found: $(\text{M}-\text{H})^-$ 1333.83; $^1\text{H NMR}$ (DMSO) δ 9.09 (s, 0.5H), 9.02 (s, 0.5H), 8.73 (d, 0.6H, $J = 7.5$ Hz), 8.11 (d, 1H, $J = 8.2$ Hz), 8.05 (m, 2H), 7.64 (m, 1H), 7.55 (t, 1H, $J = 7.5$ Hz), 7.45 (m, 2H), 7.33 (m, 4H), 7.25 (d, 1H, $J = 8.1$ Hz), 7.18 (d, 1H, $J = 2.0$ Hz), 7.11 – 6.82 (m, 4H), 4.68 (m, 1H), 4.26 (m, 2H), 3.41 (m, 4H), 3.24 (m, 6H), 2.62 (q, 2H, $J = 7.6$ Hz), 2.43 (m, 4H).

8. Solution of triethylene glycol diamine ($\text{H}_2\text{N}-(\text{CH}_2\text{CH}_2\text{O})_3-\text{CH}_2\text{CH}_2\text{NH}_2$) (47.4 mg, 0.246 mmol), carboxylic acid **6** (306 mg, 0.493 mmol), EDCI.HCl (117 mg, 0.610 mmol), HOAt (81.4 mg, 0.598 mmol) and DIPEA (0.26 mL, 1.49 mmol) in DMF (4.0 mL) was stirred for 18 h and then concentrated. Purification by silica gel chromatography (10:1 DCM:MeOH) afforded the intermediate *t*Bu ester-protected dimer (107 mg) along with **6** (159 mg). Data for *t*Bu-ester-protected dimer: $^1\text{H NMR}$ (CDCl_3) δ 8.91 (s, br, 1H), 7.58 (d, 1H, $J=7.8$ Hz), 7.31 (s, 1H), 7.25 (m, 5H), 7.16 – 7.03 (m, 6H), 6.94 (d, 1H, $J=2.1$ Hz), 6.85 (d, 1H, $J=7.5$ Hz), 4.99 (1H), 4.98 (s, 2H), 3.59 (m, 4H), 3.51 (m, 2H), 3.41 (m, 4H), 2.64 (m, 4H), 1.41 (s, 9H).

This intermediate (107 mg) was taken up in dry HCl in dioxane (4 M, 1.5 mL), stirred for 65 min, and concentrated under a stream of Ar. Purification by silica gel chromatography (90:10:0.6:0.6 CH_2Cl_2 :MeOH:H₂O:NH₄OH \rightarrow 9:1 [90:10:0.6:0.6 CH_2Cl_2 :MeOH:H₂O:NH₄OH]:MeOH) afforded dimer **8** (17.8 mg, 6% over 2 steps). Data for **8**: MS calc 1296.4 (ammonium salt), found (M-H)⁻ 1295.65; $^1\text{H NMR}$ (DMSO) δ 9.40 (s, br, 0.3H), 9.29 (s, br, 0.6H), 7.98 (m, 2H), 7.57 (dd, 2H, $J=6.9, 2.1$ Hz), 7.52 (d, 1H, $J=6.9$ Hz), 7.45 (dm 2H, $J=8.6$ Hz), 7.40 (s, 1H), 7.35 (d, 1H, $J=8.1$ Hz), 7.27 (d, 1H, $J=8.1$ Hz), 7.22 (m, 1H), 7.07 (m, 1H), 6.99 (t, 1H, $J=7.7$ Hz), 6.85 (t, 1H, $J=7.2$ Hz), 4.89 (1H, d, $J=5.0$ Hz), 4.68 (m, 2H), 4.13 (q, 4H, $J=5.1$ Hz), 2.66 (m, 2H), 2.35 (m, 4H). (Note: A residual water peak at 3.33 ppm masks peaks in that region)

2.1.5 Preparation of extended monomers

9. To a solution of indole-3-propionic acid (0.62 g, 3.3 mmol) and 6-aminohexanoic acid methyl ester* (0.60 g, 3.3 mmol) in 20 mL DMF were added EDCI.HCl (0.76 g, 4.0 mmol), HOBt (0.54 g, 4.0 mmol) and DIPEA (2.0 mL, 12 mmol) and the resulting mixture was stirred overnight. It was then diluted with EtOAc (120 mL), washed with conc. aq. NaHCO_3 (30 mL), 10% NaCl (30 mL), brine (30 mL), and concentrated. The resulting methyl ester intermediate was taken up in

4:1 THF:MeOH (30 mL) and aq. NaOH (25%, 5 mL) was added. After the reaction mixture was stirred overnight, it was quenched with aq. HCl (2.4 M, 50 mL) and extracted with EtOAc (2 x 100 mL). Combined organic extracts were washed with brine (30 mL) and concentrated affording **9** (1.22 g, 100%). Data for **9**: MS calc (M-H)⁻ 301.1552, found 301.15; NMR (CDCl₃) δ 8.37 (s, 0.9H), 7.57 (d, 1H, J = 7.8 Hz), 7.33 (d, 1H, J = 7.3 Hz), 7.16 (m, 1H), 7.09 (m, 1H), 6.97 (s (br), 1H), 5.59 (s, 0.9H), 3.11 (br, 4H), 2.57 (br, 2H), 2.26 (t, 2H, J = 7.4 Hz), 1.53 (br, 2H), 1.31 (br, 2H), 1.14 (br, 2H).

10. To a solution of carboxylic acid **9** (75.4 mg, 0.249 mmol) and amine **3a** (149 mg, 0.276 mmol) in 2.0 mL dry DMF were added EDCI.HCl (56.5 mg, 0.29 mmol), HOAt (41.8 mg, 0.31 mmol) and DIPEA (0.13 ml, 0.75 mmol) and the resulting mixture was stirred for 48 h. It was then diluted with EtOAc (30 mL), washed with conc. aq. NaHCO₃ (15 mL), 10% NaCl (15 mL), brine (15 mL), and concentrated. Purification by silica gel chromatography (4:1 EtOAc:hexanes → EtOAc) afforded *t*Bu ester-protected intermediate (205 mg, 100%). R_f = 0.30 (4:1 EtOAc:hexanes).

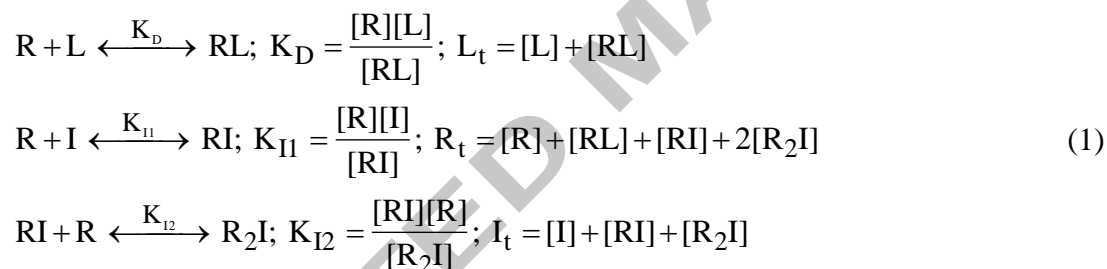
This intermediate (153 mg) was taken up in dry HCl in dioxane (4 M, 2.5 mL), stirred for 2 h, and concentrated. Purification by silica gel chromatography (10:1 DCM:MeOH) afforded **10** (31.8 mg, 22%). Data for **10**: R_f = 0.18 (9:1 DCM:MeOH); MS calc: 766.88, found (M-H)⁻ 765.48; ¹H NMR (acetone) δ 8.34 (s, 0.4H), 8.32 (s, 0.5H), 8.15 (s, 0.7H), 7.67 (m, 2H), 7.56 (d, 1H, J = 7.8 Hz), 7.47 (s (br), 1H), 7.41 (m, 2H), 7.35 (d, 2H, J = 8.2 Hz), 7.27 (br, 2H), 7.18 (t, 1H, J = 5.5 Hz), 7.12 – 6.96 (m, 7H), 4.99 (m, 1H), 4.29 (t, 2H, J = 6.2 Hz), 3.52-3.35 (m, 2H), 3.24 (t, 2H, J = 6.4 Hz), 3.18 (q, 2H, J = 6.4 Hz), 3.07 (t, 2H, J = 7.6 Hz), 2.56 (t, 2H, J = 7.6 Hz), 2.14 (t, 2H, J = 7.6 Hz), 1.53 (t, 2H, J = 7.6 Hz), 1.43 (t, 2H, J = 7.6 Hz), 1.25 (m, 2H).

11. To a solution of carboxylic acid **9** (60.0 mg, 0.198 mmol) and amine **4a** (102 mg, 0.2 mmol) in 2.0 mL dry DMF were added EDCI.HCl (58.4 mg, 0.305 mmol), HOAt (33.4 mg, 0.245 mmol) and DIPEA (0.10 ml, 0.57 mmol) and the resulting mixture was stirred overnight. It was then diluted with EtOAc (30 mL), washed with conc. aq. NaHCO₃ (15 mL), 10% NaCl (15 mL), brine (15 mL), and concentrated. Purification by silica gel chromatography (19:1 DCM:MeOH) afforded *t*Bu ester-protected intermediate (141 mg, 89%). R_f = 0.24 (10:1 DCM:MeOH). This intermediate (78.5 mg) was taken up in dry HCl in dioxane (4 M, 1.5 mL), stirred for 2 h, and concentrated. Purification by silica gel chromatography (9:1 DCM:MeOH) afforded **11** (45.7 mg, 63%). Data for **11**: R_f = 0.18 (9:1 DCM:MeOH); MS calc. 748.27, found (M-H)⁻ 746.44 ¹H NMR (acetone) δ 10.01 (s, br, 0.3H), 9.87 (s, br, 0.6H), 8.51 (s, 0.7H), 8.32 (d, 1H, J=8.0 Hz), 7.67 (d, 1H, J=7.7 Hz), 7.55 (m, 2H), 7.46 (m, 3H), 7.43-7.31 (m, 6H), 7.27 (s, 1H), 7.10-6.95 (m, 5H), 5.02 (m, 1H), 3.50 (dd, 2H, J=14.4, 4.8 Hz), 3.37 (m, 2H), (m, 2H), 3.04 (t, 2H, J=7.2 Hz), 2.52 (t, 2H, J=7.8 Hz), 2.37 (t, 2H, J=7.4 Hz), 2.22 (q, 2H, J=5.8 Hz), 1.62 (t, 2H, J=7.4 Hz), 1.44 (t, 2H, J=7.4 Hz), 1.29 (m, 2H).

2.2 Assays

2.2.1 Fluorescence binding assay Inhibition constants K_i for binding in the hydrophobic pocket were determined using a fluorescence intensity assay as previously described.¹⁴ Fe^{II}(env2.0)₃ was used to mimic the hydrophobic pocket in the gp41 NHR coiled coil. Env2.0 has the sequence bpy-GQAVEAAQQHLLQLTVWGIKQLQARILAVEKK-amide, where bpy is 2,2-bipyridine-5-carboxylate, a bidentate ferrous iron chelator that assures the trimeric structure of the NHR upon metal binding. Underlined residues occur in WT HXB2 gp41. C-peptide C18e2.0-FL (Ac-MTWBEWDREIBNYTSLIC, B = α-aminoisobutyric acid, WT residues underlined) labeled with fluorescein at the cysteine residue, was used to probe inhibitor binding.

Quenching of C18e2.0-FL occurred upon addition of $\text{Fe}^{\text{II}}(\text{env}2.0)_3$, with a $K_D = 0.8 \mu\text{M}$ and a minimal fractional fluorescence for the complex = 0.072. K_I was determined by measuring the dose dependent fluorescence recovery in the presence of a competitive inhibitor. $7.2 \mu\text{M}$ $\text{Fe}(\text{env}2.0)_3$ (measured as concentration of HP binding sites, with three equivalent sites per trimer) and 30 nM C18e2.0FL were used in the competitive inhibition experiments, with serial dilution of the inhibitors in the range $0.39 - 400 \mu\text{M}$, in Tris-acetate buffer at pH 7.0 and 4% DMSO.²⁵ Concentration of dimeric inhibitors was calculated as one molecule per dimeric unit. 12 points per binding curve were measured in triplicate for each compound. Fractional fluorescence data were fit to equations (3) and (4) for 1:1 ligand : HP binding (Section 3.3). For 1:2 ligand : HP binding, data were fit by numerical solution (Mathcad, Mathsoft) of the equation



where L_t , R_t and I_t are the concentrations of probe, HP binding sites in receptor $\text{Fe}(\text{env}2.0)_3$, and inhibitor, respectively, K_{I1} and K_{I2} are the inhibition constants for the first and second binding interactions. The observed fractional fluorescence was calculated from equation (3).

The fit of calculated to observed data was determined from the sum of squares (equation (2)):

$$\text{SSQ} = \sum_{i=1}^{12} \{ \max(|F_{\text{obs},i} - F_{\text{calc},i}| - \sigma_i, 0) \}^2 \tag{2}$$

where $F_{\text{obs},i}$ and $F_{\text{calc},i}$ are the fractional fluorescence and s_i is the standard deviation of each data point.

2.2.2 Surface Plasmon Resonance Experiments Experiments were carried out on a Biacore T100 instrument. A CM5 sensor chip surface was activated by injecting 360 μl EDC/NHS (freshly prepared by mixing 5 mM EDC and 5 mM NHS (1:1 v/v) in biacore HBS-EP buffer), followed by introduction of 150 μl PDEA (80 mM in 0.1 M sodium borate buffer, pH 8.5) at a flow rate of 20 $\mu\text{l}/\text{min}$. The bioreceptor $\text{Fe}^{\text{II}}(\text{envC})_3$ (envC = bpy-GQAVEAQQHLLQLTVWGIKQLQARI(d)C-amide, WT HXB2-Env residues underlined) was then bound to the sensor chip surface by injecting 150 μl (5 μM $\text{Fe}^{\text{II}}(\text{envC})_3$ in 25 mM Tris-acetate buffer, pH 7.0) for 2 – 9 minutes at 10 $\mu\text{l}/\text{min}$. Unreacted disulfide surface was deactivated with 50 μl L-cysteine (50 mM in 0.1 M sodium acetate buffer, 1 M NaCl, pH 4.5) followed by a wash with 200 μl of freshly prepared 1 mM ferrous ammonium sulfate at 20 $\mu\text{l}/\text{min}$, to ensure that any ferrous ion leached at low pH was restored. Any non-specifically bound material was removed with 50 μl of 500 mM NaCl at 50 $\mu\text{l}/\text{min}$. An equivalent reference surface was generated using the same procedure as above excluding the $\text{Fe}^{\text{II}}(\text{envC})_3$ coupling step. Analytes were detected at serially increasing concentrations from 0.098 to 50 μM in HEPES buffered saline (20 mM HEPES, 150 mM NaCl) at pH 7.0 containing 1% DMSO, using a 60 s association time and 300 s dissociation time. DMSO bracketing was used to correct the refractive index. Analysis of sensorgram data was carried out with Biacore BIAevaluation software.

2.2.3 Cell-cell Fusion Assay Cell-cell fusion was measured using cell lines obtained through the NIH AIDS Research and Reference Reagent Program, Division of AIDS, NIAID, NIH. Target cells were TZM-bl cells (#8129, contributed by J.C. Kappes, X. Wu and Tranzyme Inc.)

expressing CD4, CCR5 and CXCR4,²⁶ and containing an integrated reporter gene for firefly luciferase under control of HIV-1 LTR.²⁷ Effector cells were HL2/3 (#1294, contributed by B.K. Felber and G.N. Pavlakis) which produce HXB2 Env, Tat and Rev.²⁸ Serially diluted inhibitors were added to 96 well plates containing 25,000 TZM-bl cells per well cultured overnight. 50,000 HL2/3 cells were added per well, and fusion allowed to proceed for 6 hours in reduced serum medium (Gibco) with a final concentration of 1% DMSO. Luciferase expression was measured using Luciferase Assay Reagent (Promega) according to the manufacturer's instructions. Controls containing 1% DMSO with and without HL2/3 cells were measured for each compound, and experiments were performed in triplicate.

2.2. 4 Viral Replication and Attachment Assays Inhibition of HIV-1 replication was determined in CCR5- and CXCR4-tropic MAGI antiviral assays and inhibition of HIV-1 attachment/entry was determined in CCR5-tropic MAGI attachment assays as previously described.^{29, 30} HIV-1 isolates and cells were obtained from the NIH AIDS Research and Reference Reagent Program, Division of AIDS, NIAID, NIH, as follows: HIV-1 Ba-L from Suzanne Gartner, Mikulas Popovic, and Robert Gallo.^{30, 31} HIV-1 IIIB from Robert C. Gallo.^{30, 32} MAGI-CCR5 cells from Dr. Julie Overbaugh.^{33, 34} For MAGI antiviral assays, MAGI-CCR5 cells were grown overnight in 96 well plates in DMEM supplemented with 10% FBS, using 10,000 cells per well. The following day the medium was removed and compounds diluted in medium were added (6 dilutions in triplicate at each dilution), followed by the addition of either HIV-1 Ba-L (CCR5-tropic assay) or HIV-1 IIIB (CXCR4-tropic assay) at approximately ten 50% tissue culture infective doses per well (~10 TCID₅₀/well). Assay plates were incubated for 48 hours, after which medium was removed and HIV-1 Tat-induced β -Gal enzyme expression was determined by chemiluminescence using Tropix Gal-Screen (Applied Biosystems)

according to the manufacturer's instructions. MAGI attachment assays were performed similarly, but with a washout of unbound virus and compounds three (3) hours post-infection. Assays were conducted at a serum concentration of 2%.

2.2.5 Cytotoxicity Assay The cytotoxic effect of the compounds was determined using the identical cell culture procedure to that described above for viral replication or cell-cell fusion, but measuring cell viability, using 3-(4,5-dimethylthiazol-2-yl)-5-(3-carboxymethoxyphenyl)-2-(4-sulfophenyl)-2H-tetrazolium (MTS, CellTiter 96 reagent; Promega; used for MAGI assays) or using a resazurin cell viability reagent (Alamar Blue or Presto Blue, Life Technologies; used for cell-cell fusion assays) following the manufacturers' protocols.

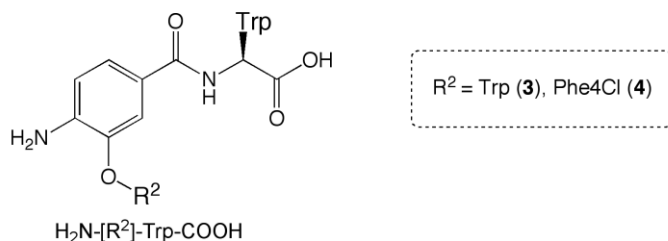
2.3 Computational docking

Ligand charges and low energy conformations were obtained using OpenEye software^{35,36} (fixpka, molcharge, omega2-2.5.1.4 and szybki, OpenEye Scientific Software, Santa Fe, NM. <http://www.eyesopen.com>). Compounds were docked into pdb structure 3P7K using Autodock Vina. A model of bivalent binding of the dimer **7** (Figure 3) was obtained using low energy conformers of two partial structures, split at the edge of the PEG₃ linker. Structures were docked and linker dihedrals were manually adjusted to reconnect the two parts. The local geometry was then optimized and clashes removed using the default minimization protocol in Chimera (UCSF) (Potential energy of complex -12.4×10^3 , RMSD 0.0244 Å over 2460 atoms).

3. Results

3.1 Synthesis and Description of Compounds Six compounds were prepared as shown in Figure 2 and Schemes 1 - 3. There were two series, based on the two-subunit peptidomimetic compounds **3** (H₂N-[Trp]-Trp-OH) and **4** (H₂N-[Phe4Cl]-Trp-OH), designated "monomers".

Monomers - two subunit peptidomimetics



Monomer extensions

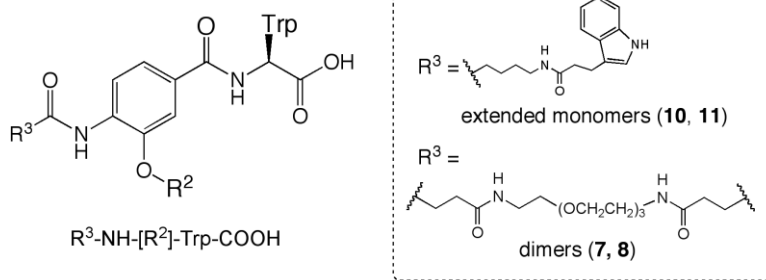
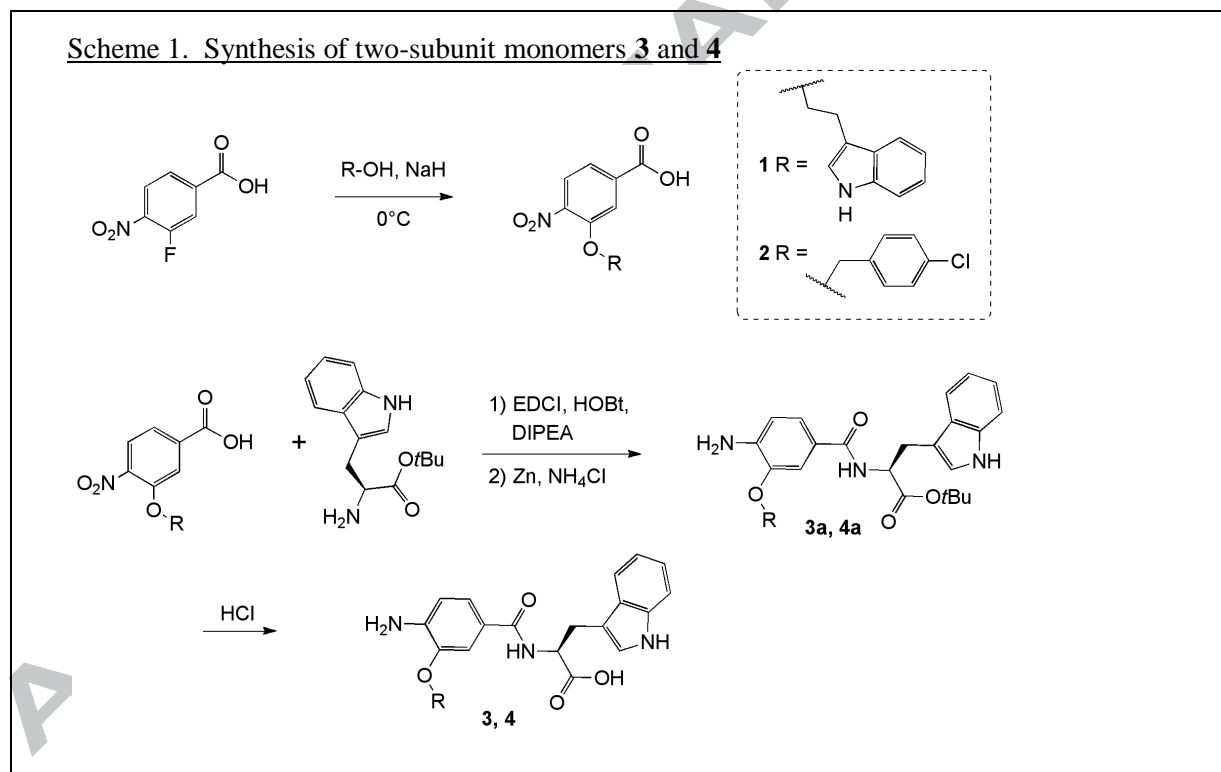


Figure 2. Structures of peptidomimetic inhibitors used in this study

Scheme 1. Synthesis of two-subunit monomers **3** and **4**

Dimers **7** and **8** had two peptidomimetic monomers connected by a 22.5Å succinate-PEG₃-succinate spacer (PEG₃ = triethylene glycol), calculated to be sufficiently long to permit simultaneous binding into two hydrophobic pockets of the HR1 trimer. A model of **7** produced

by docking into the HR1 trimer and energy minimization (see Materials and Methods) is shown in Figure 3. The two monomers reach into two HP's of the trimer with the PEG linker units in mostly all trans conformation. Extended monomers **10** and **11** were substituted at the aniline with a hydrophobic alkyl tail terminated by a Trp, with the goal of increasing interactions within the HR1 groove beyond the HP. LC-MS and NMR figures of the final compounds are shown in Supplementary Data Figures S1 and S2.

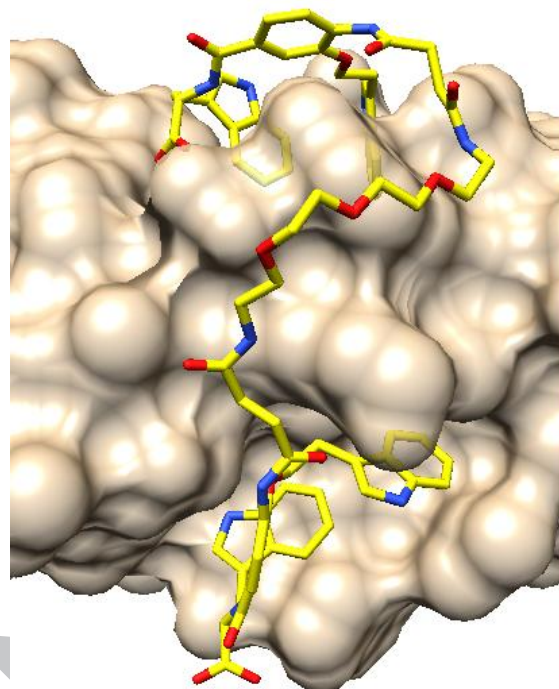


Figure 3. Model showing the ability of dimer **7** to reach around the HR1 coiled coil with the terminal -NH-[Trp]-Trp-OH units interacting in two hydrophobic pockets. The surface representation of the HR1 (pdb 3P7K) has been made partly transparent to reveal the docked aromatic rings of **7**.

3.2 Anti-fusion activity improved with compound

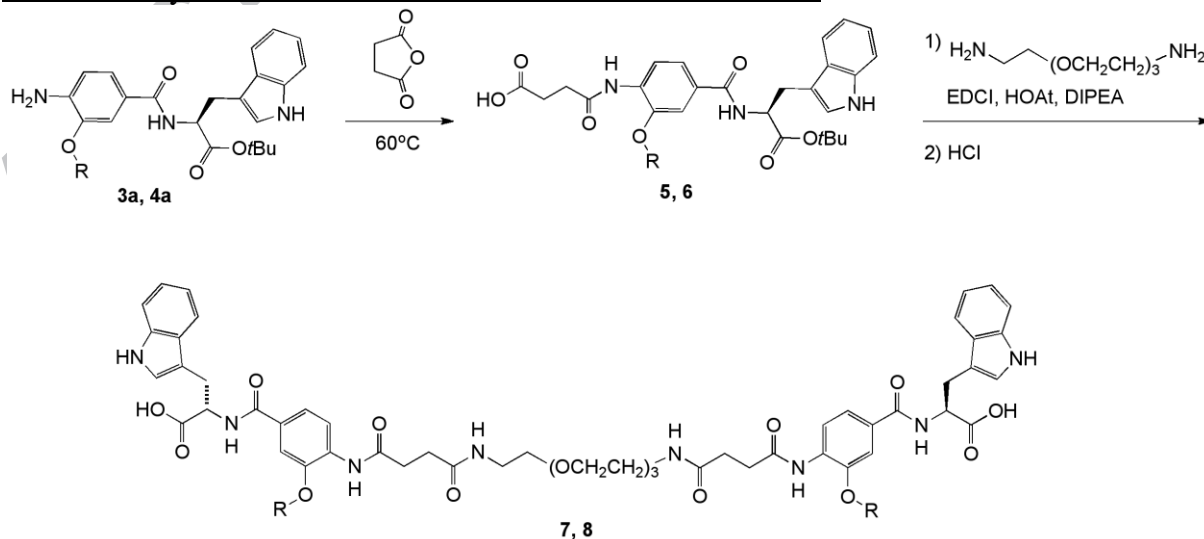
elaboration Activity of the two series of

compounds was investigated in cell – cell fusion

(CCF) assays using effector cells expressing CXCR4-tropic_HXB2-Env, and in virus – cell

fusion (VCF) assays using laboratory adapted strains Ba-L (CCR5-tropic) and IIIB (CXCR4-

Scheme 2. Synthesis of dimers **7** and **8** from monomers **3** and **4**



tropic). The results are shown in Figure 4 and Table 1. CCF was inhibited more readily than VCF, and augmenting the basic monomer significantly improved anti-fusion activity. None of the compounds exhibited any toxicity at the concentrations tested.

Scheme 3. Addition of a hydrophobic tail to monomers 3 and 4, forming 10 and 11

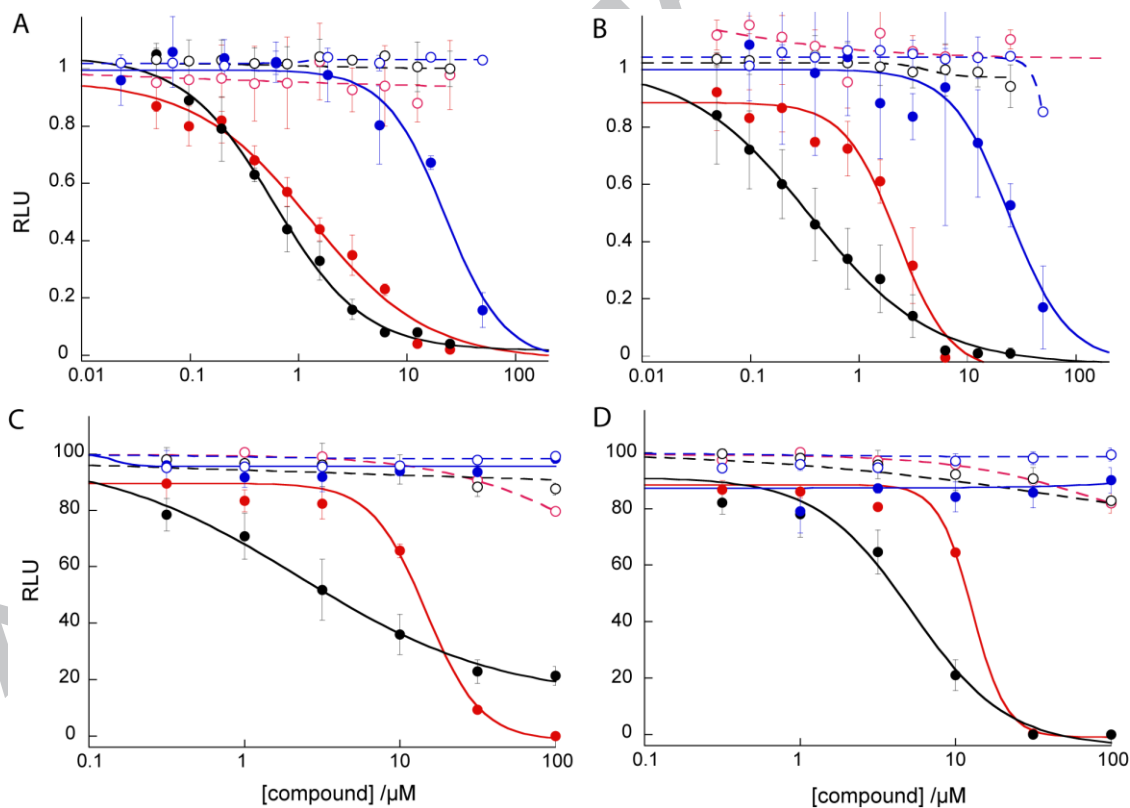
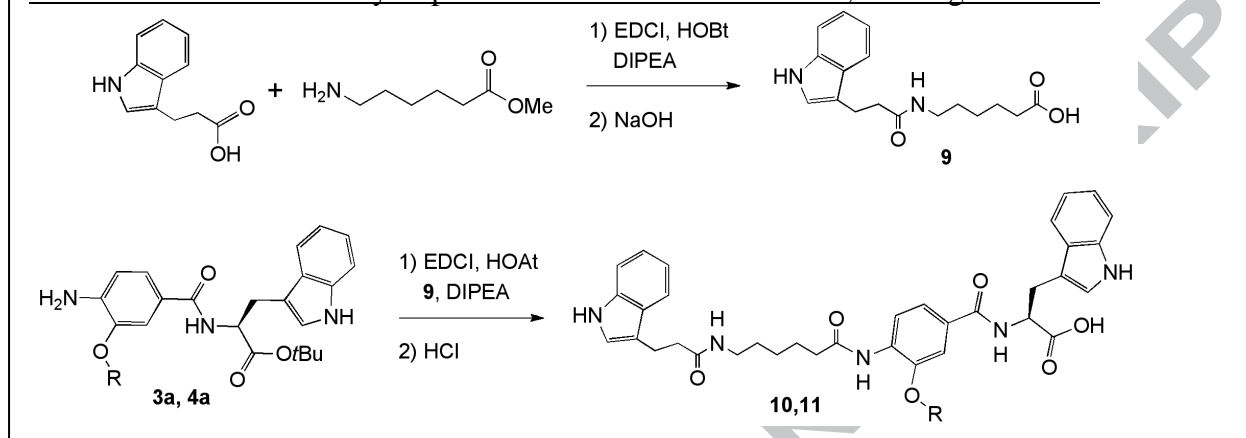


Figure 4. Dose-response curves for each compound demonstrating percent inhibition of cell-cell fusion (A, B) and Ba-L viral infectivity (C, D) measured as relative luminescence units (RLU) using a luciferase reporter. A, C. Compounds 3 (blue), 7 (black), 10 (red); B, D. Compounds 4 (blue), 8 (black) and 11 (red). Cell viability is shown in corresponding open circles. Error bars are standard deviations of three measurements.

Table 1. Activity data against HIV-Env mediated fusion*

Compounds	cell-cell fusion		virus- cell fusion				CC ₅₀
	HXB2		Ba-L		IIB		
	IC ₅₀	IC ₉₀	IC ₅₀	IC ₉₀	IC ₅₀	IC ₉₀	
3	22	80	> 50	> 50	> 50	> 50	> 50
10	1.3	15.1	13.7	31.1	17.3	30.5	> 100
7	0.6	6.3	3.6	>100	3.8	70.0	> 100
4	24	49	> 50	> 50	> 50	> 50	> 50
11	2.2	5.6	13.0	26.5	14.3	27.1	> 100
8	0.4	4.4	4.7	18.3	5.1	20.8	> 100

*3-6 repeats of each measurement, error is 10-20%, in μM

Monomers H₂N-[Trp]-Trp-OH and H₂N-[Phe4Cl]-Trp-OH were weak CCF inhibitors (22 – 24 μM) and were ineffective against VCF. Activity improved to 1 -2 μM against CCF and 13 – 17 μM against VCF with addition of the hydrophobic tail in compounds **10** and **11**. Many studies indicate that increased hydrophobic character is consistent with increased fusion inhibitory activity,³⁷ including the preference for aromatic side chains at positions R¹, R² (and R³) of this peptidomimetic library (Figure 2). The added hydrophobic tail with the terminal Trp may interact in the HR1 groove of the hydrophobic gp41 protein, or may associate with the lipid bilayer, orienting and concentrating the ligand in the biological milieu of the fusion reaction.

Dimerization of the inhibitors with a 22Å PEG linker connecting two monomers resulted in the best performing member of each series, with compounds **7** and **8** having IC₅₀'s < 1 μM against CCF and 3-5 μM against VCF. In this case, it is not expected that the PEG linker would interact extensively with the membrane,²⁰ suggesting that additional HR1 interactions could form the basis of the improved activity. We noted that the antiviral activity of **7** reached a plateau at ~20% residual fusion activity of Ba-L virus and ~6% residual fusion activity of IIB virus. The faster kinetics of Ba-L fusion may limit the potency of the largest molecular weight inhibitor **7**.

3.3 Solution binding studies confirmed hydrophobic pocket binding Next we wished to ascertain whether the 50-fold increase in potency was a cooperative effect of dimers binding into two HP's of one HR1 trimer, as designed. We therefore examined whether binding and kinetic data could discriminate between a monovalent and bivalent binding mechanism. Affinity of the compounds for the gp41 HP was determined by fluorescence using a competitive inhibition assay that has been previously described.^{14,25} Briefly, the hydrophobic pocket (receptor R) is formed by metal ion assisted association between three HR1 peptides env2.0 spanning the pocket sequence (HXB2 residues 560 – 584) that are covalently linked to N-terminal 2,2'-bipyridine (bpy). Ferrous ion binding in 1/3 stoichiometry to peptide results in spontaneous formation of an HR1 trimeric coiled coil as a magenta-colored complex Fe(env2.0)₃. The fluorescence of HR2 probe peptide (HXB2 residues 626-642) labeled with fluorescein at the C-terminus (L = C18-e2.0FL) is quenched upon binding to Fe(env2.0)₃, forming the basis of the fluorescence assay. Compounds binding to the HP displace the probe peptide with a concomitant increase in fluorescence. Inhibition constants (K_I) are determined by dose response measurements. Data were fit to the equation

$$F_{\text{obs}} = F_{\text{RL}} + (F_{\text{L}} - F_{\text{RL}}) \frac{K_{\text{D}}}{K_{\text{D}} + [\text{R}]} \quad (3)$$

where K_D is the dissociation constant of the Fe(env2.0)₃-C18-e2.0FL complex, and F_L and F_{RL} are the fluorescence of free and bound C18-e2.0FL. Known parameters are K_D = 0.8 μM and fractional F_{RL} = 0.072.¹⁴

For 1:1 binding of ligand with HP's on the trimer Fe(env2.0)₃, the concentration of free HP, [R], was calculated analytically according to the equation

$$[\text{R}] = \{R_{\text{t}} - I_{\text{t}} - K_{\text{I}} + \sqrt{(R_{\text{t}} - I_{\text{t}} - K_{\text{I}})^2 + 4R_{\text{t}}K_{\text{I}}}\} / 2 \quad (4)$$

R_t , I_t and L_t are the total concentrations of added receptor binding sites, inhibitor and probe peptide respectively, and K_i is the inhibition constant. Equation (4) is an analytical approximation valid when $R_t \gg L_t$ which is fulfilled by the experimental conditions. Equation (3) was also solved numerically for both 1:1 and 1:2 binding models, requiring no approximations (Materials and Methods). The analytical approximation of 1:2 binding of ligand to two HP's required solution of a cubic equation and was not used.

3.3.1 Avidity for the HP did not predict the order of observed biological activity In

previous studies, we have shown a correlation between low μM binding to $\text{Fe}(\text{env}2.0)_3$ and inhibition of HIV-fusion.^{5, 6, 23} Competitive inhibition dose response curves for **3**, **4**, **7**, **8**, **10** and

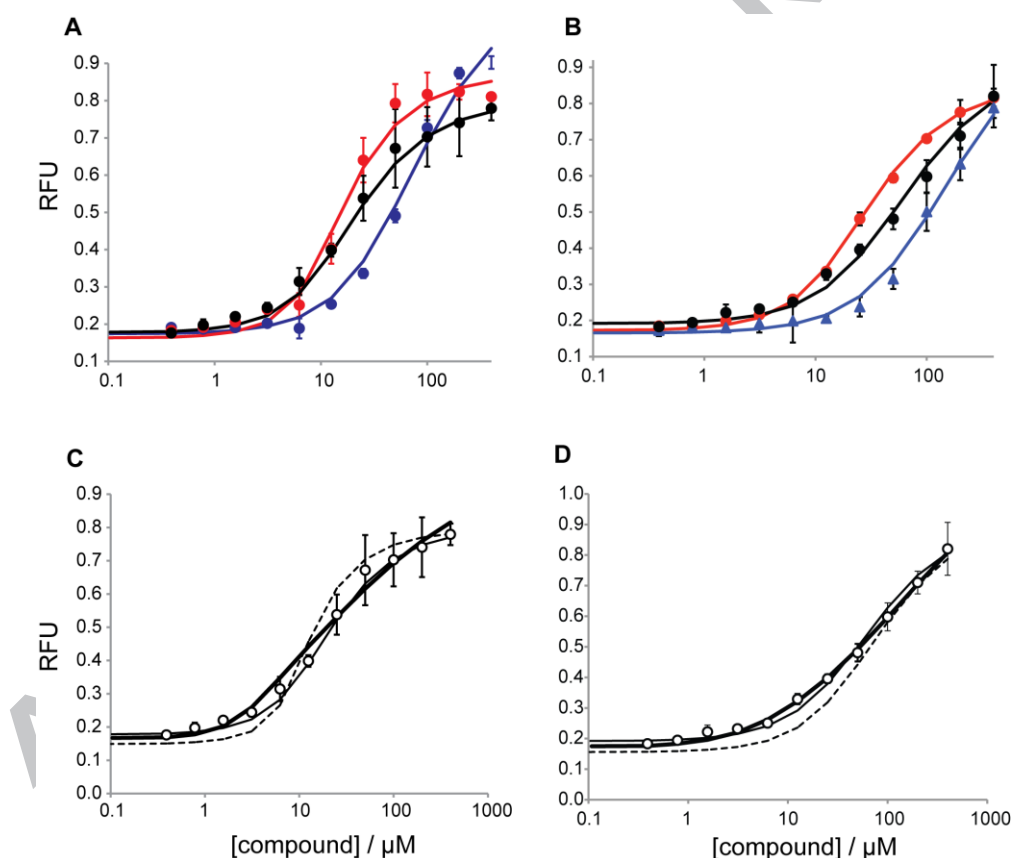


Figure 5. Fluorescence competitive inhibition dose response curves performed with $7.2 \mu\text{M}$ binding sites. A. **3** (blue), **7** (black), **10** (red) and B. **4** (blue), **8** (black), **11** (red). C and D show data fitting for dimers **7** and **8** to a 1:1 binding model (dashed line) and 1:2 binding model (bold solid line) assuming $7.2 \mu\text{M}$ binding sites. The narrow solid lines show an alternative fit to a 1:1 binding model with 40% reduced receptor concentration. RFU = relative fluorescence units, as a fraction of the fluorescence of probe plus compound in the absence of receptor (F_L).

11, conducted using 7.2 μM R_t and 30 nM L_t , are shown in Figure 5A and 5B. Here too, we observed that low μM inhibition in the binding assay was commensurate with activity against HIV-Env mediated fusion; however it was not completely correlated. A higher concentration was required for 50% activity of dimer compared to the corresponding extended monomer in the fluorescence assay, while dimers were clearly more potent in biological assays. Additionally, the slope of the binding curves was lower for the bivalent inhibitors. Parameters F_L , R_t and K_I were determined from dose response curves by fitting to equations 1 and 2, and / or by numerical simulation. Results are given in Table 2.

Compound	Binding model [‡]	F_L	R_t (μM)	Inhibition constant (μM)	SSQ / 10^{-3}
3 (monomer)	1:1	1.08	7.2	$K_I = 7.2 \pm 1.1$	2.13
10 (extended monomer)	1:1	0.85	6.2	$K_I = 1.2 \pm 0.2$	2.07
7 (dimer)	1:1	0.79	7.2	$K_I = 1.0 \pm 0.3$ §	10.11
	1:1	0.80	4.3	$K_I = 2.3 \pm 0.3$	0.014
	1:2	0.95	7.2	$K_{I1} = 20, K_{I2} = 0.2$	0.928
4 (monomer)	1:1	1.00	7.2	$K_I = 15 \pm 2.6$	0.258
11 (extended monomer)	1:1	0.85	5.5	$K_I = 3.4 \pm 0.18$	0.066
8 (dimer)	1:1	0.99	7.2	$K_I = 5.3 \pm 1.5$ §	18.7
	1:1	0.90	4.5	$K_I = 8.5 \pm 1.3$	0.596
	1:2	1.05	7.2	$K_{I1} = 21, K_{I2} = 1.3$	0.168

† Data were fit to equations (3) and (4) or (1), and the sum of squares SSQ was calculated using equation (2), see text. ‡ The binding model is defined as the ratio of ligand : HP. § Poor fit. The total HP concentration in the assay, R_t , was 7.2 μM . Maximum fractional fluorescence $F_L < 1$ could be due to light scattering

3.3.2 Monomers and extended monomers could be fit to a 1:1 binding model Fluorescence data for monomers **3** and **4** were simulated by a 1 ligand : 1 HP binding model, with the expected concentration of HP, $R_t = 7.2 \mu\text{M}$. Fits to the data for extended monomers **10** and **11** yielded R_t values that were 14-20% lower than those of the corresponding monomer, which we interpreted as an outcome of the low solubility of these hydrophobic inhibitors, causing

aggregation of the receptor – compound complex. Consequently, the aggregates caused light scattering in the fluorescence assay, leading to values for $F_L < 1$ (Table 2). [Trp]-Trp containing peptidomimetic compounds **3** and **10** were measurably more potent than [Phe4Cl]-Trp compounds **4** and **11**, consistent with their higher hydrophobic character. Observed inhibition constants were 7 μM for **3**, 15 μM for **4**. Adding the hydrophobic tail improved HP binding affinity by a factor of 5 to 6, to 1.2 for **10** and 3.1 for **11**, mirroring the results obtained in fusion inhibition studies and further consolidating the role that hydrophobic character and HP binding play in compound activity.

3.3.3 The data are compatible with a bivalent interaction of dimers with $\text{Fe}(\text{env}2.0)_3$ Using the experimental value of $R_t = 7.2 \mu\text{M}$, fluorescence data for the bivalent inhibitors **7** and **8** could not be fit to a 1:1 binding model. Instead, data fitting supported a model in which simultaneous binding of one bivalent ligand into two hydrophobic pockets occurred (Table 2, Figure 5C, D, Figure 6). Since there are three HP's per trimer, the simplest model for full occupancy of the HP's would include a bidentate bound dimer and a monodentate bound dimer (Figure 6). This leaves only 67% of receptor binding sites available for the total number of dimer molecules. An excellent fit to the data was in fact achieved using a 1:1 binding model with ~40% reduction in R_t . These fits yielded K_I 's of 2.3 μM and 8.5 μM for **7** and **8**, respectively, 2 – 3 fold improved over the respective monomers. The observed K_I 's are assumed to be an average over monodentate and bidentate binding. Best fit R_t values at ~60% implicate some aggregation as part of this model fitting, supported by the observation of F_L values < 1 .

The data could also be fit with the full complement of $R_t = 7.2 \mu\text{M}$ using a model of 1:2 binding of one bivalent ligand : 2 HP's. Notably the binding constant for the first interaction, $K_I = 20$ to 21 μM , was higher than the K_I for the monomers **3** or **4**, and likely reflects an entropic

penalty due to the flexible PEG linker, while K_{12} for the second interaction at the other end of the PEG linker was more than an order of magnitude lower than for the monomers, implying a cooperative binding effect or a local concentrating effect due to the first interaction. There was no evidence of aggregation from the F_L values. The mathematical modeling does not specify whether the HP's are on the same or different trimers, since they are each considered independent and identical. It is unlikely that a ligand with the limited potency of **7** or **8** could bridge two trimers in solution. Since the data fitting required every available HP, it is likely that a second bivalent inhibitor in the third site of each trimer engages in an equilibrium exchange for bidentate binding with the first bivalent inhibitor, as illustrated in Figure 6. Data resolution does not permit us to distinguish this dynamic model from the static scenario described above.

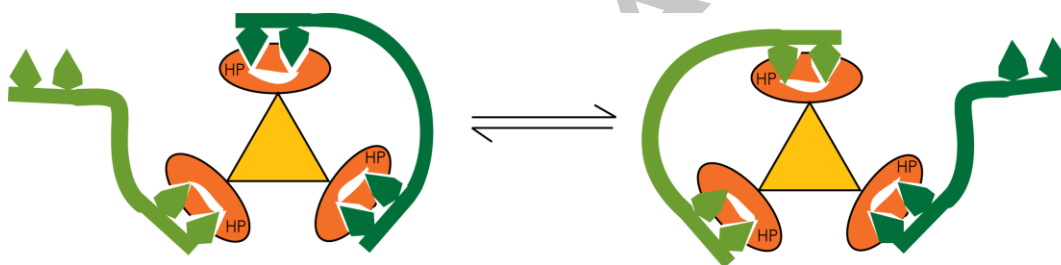


Figure 6. A model of bidentate binding of dimers to the HR1 trimer. The HP's, shown in orange, are arranged on a three-fold axis of symmetry. Each green diamond shape represents an aromatic side chain of the 2-subunit peptidomimetic monomer. Two equivalent dimers are depicted in green and light green.

A third option for data fitting involves monodentate binding for all of the dimers, with a significant degree of receptor aggregation occurring during the assay. We cannot formally rule out this possibility, given that the inhibitors are quite hydrophobic. We therefore turned to surface binding studies to evaluate inhibitor interactions.

3.4 Surface binding studies yielded kinetics of binding Hydrophobic pocket binding was evaluated using surface plasmon resonance (SPR) to measure association and dissociation kinetics. Analysis of the fluorescence data and previous literature observations¹² suggested that bivalent binding should display an altered kinetic profile compared to 1:1 binding, permitting us

to verify our interpretation of the solution equilibrium binding studies. Furthermore, we were curious to know whether kinetics, especially off-rate could be correlated more effectively to observed biological potency than K_I , given that the target is a transient intermediate structure. Previous studies have shown that on-rate can limit the effectiveness of a large protein inhibitor,³⁸ and high potency is accompanied by a slow off-rate.^{21, 39}

SPR experiments were conducted on a Biacore CM5 chip using a modified version of the receptor peptide Fe(envC)₃. The peptide envC is terminated by a D-cysteine residue, which orients the thiol group along the axis of the peptide and permits vertical anchoring of the receptor to the surface groups. We have previously used this receptor in electrochemical and SPR binding studies of peptide and small molecule – gp41 HP interactions.⁴⁰ The design creates a homogeneous ligand surface with open binding sites on the three faces of the three-fold symmetrical receptor, such that dimers could simultaneously bind into two pockets, if that is indeed their mechanism.

We achieved immobilization responses in the range 2460 – 5670 units, corresponding to approximately one Fe(envC)₃ molecule per 32.6 – 8.3 nm², respectively, or effective concentrations between 2.6 – 6 mM.^{41, 42} A reference channel was prepared without receptor, and signals from this channel were subtracted out to yield SPR sensorgrams that reflected interactions with Fe(envC)₃. Specificity of analyte binding was confirmed by observing both analyte and Fe(envC)₃ concentration dependent responses (Supplementary Data, Figure S3). Typically, below ~10 μM, analyte responses were well below 100 RU, suitable for kinetic analysis. At higher concentrations, most compounds gave disproportionately high analyte responses, likely due to non-specific binding or aggregation. These sensorgrams were not included in the analysis.

We measured the association rate (k_a), dissociation rate (k_d) and rate constant ($K_D = k_d/k_a$) for each compound at various concentrations, by analyzing sensorgrams using Langmuir 1:1 binding and 1:2 binding kinetic analysis. The maximum analyte response, RU_{max} , occurring at saturating concentrations of analyte, was not obtained experimentally due to non-specific aggregation, and was determined from a good fit to SPR data for compound **7**. Remaining sensorgrams were fit by fixing RU_{max} proportionately according to the molecular weight of the analyte. Uncertainty in RU_{max} led to ~30% uncertainty in k_a , but still allowed us to compare kinetics within the compound set. Off-rate k_d was less dependent on RU_{max} . The results are reported in Table 3, shown for the [Phe4Cl]-Trp series in Figures 7 and for the [Trp]-Trp series in Supplementary Data Figure S4. The data clearly reveal significantly slower kinetics for bivalent compounds **7** and **8** compared to monovalent compounds **3** and **4**, with intermediate rates observed for the extended monomers **10** and **11**. Monomers **3** and **4** had fast on- and off-rates, on the order of $k_a \sim 6 * 10^4 \text{ M}^{-1}\text{s}^{-1}$ and $k_d \sim 0.8 \text{ s}^{-1}$. Both on-rate and off-rate for dimers were an order of magnitude slower, with $k_a \sim 3000 \text{ M}^{-1}\text{s}^{-1}$, and $k_d \sim 0.05 \text{ s}^{-1}$. The slow on-rate is likely due to the increased size and flexibility of the dimers, while the slow off-rate is consistent with dual binding interactions with $\text{Fe}(\text{envC})_3$ where there is a higher probability of rebinding before the partner can dissociate. The extended monomers **10** and **11** have a large hydrophobic

	$k_a \text{ (M}^{-1}\text{s}^{-1}\text{)}$	$k_d \text{ (s}^{-1}\text{)}$	$k_d/k_a \text{ (M)}$	RU_{max}^*	$\chi^2 \text{ (RU}^2\text{)}$
3 (monomer)	5.10e4	0.834	1.6e-5	59	4.54
10 (ext. monomer)	1.10e4	0.093	1.4e-5	95	5.58
7 (dimer)	0.37e4	0.060	1.6e-5	160	2.62
4 (monomer)	6.70e4	0.820	1.2e-5	56	5.45
11 (ext. monomer)	1.37e4	0.186	1.4e-5	93	2.90
8 (dimer)	0.18e4	0.037	2.1e-5	157	1.68

* RU_{max} was fixed during global curve fitting of sensorgrams at 3, 4 or 5 concentrations for monomers, extended monomers or dimers, respectively

binding capacity and a flexible hydrophobic tail, which translated into intermediate values for k_a and k_d compared to the monomers and dimers, as well as lower K_I 's observed by fluorescence. Changes of the same order of magnitude in both k_a and k_d resulted in little discrimination in K_D over the dataset. Values for K_D obtained by the SPR experiment are of limited accuracy due to

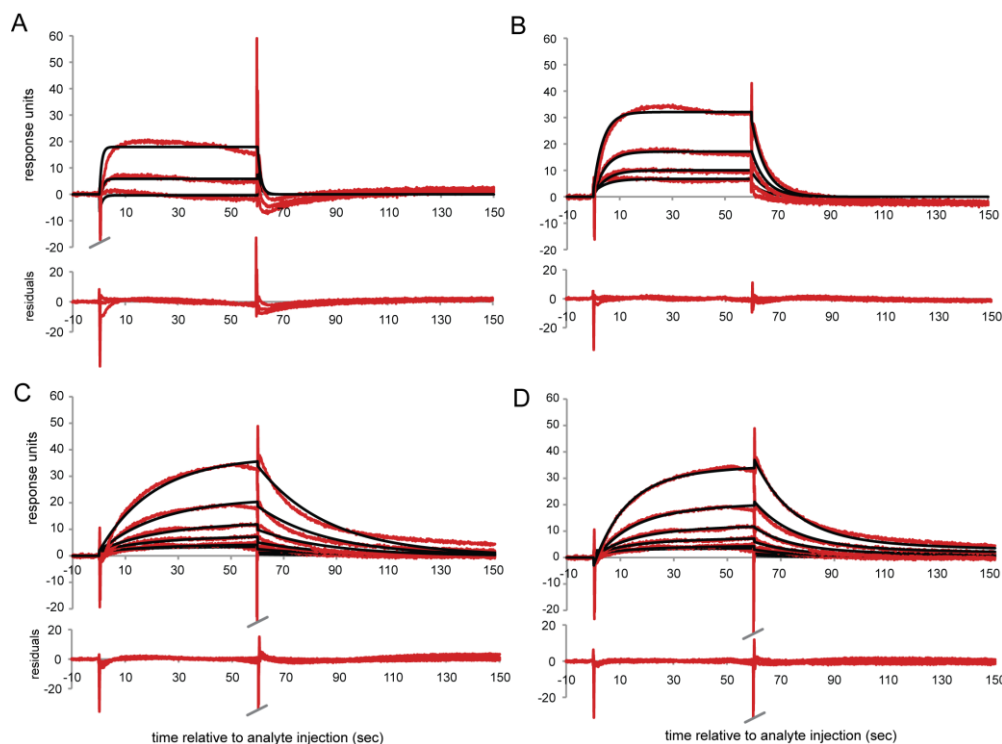


Figure 7. SPR sensorgrams obtained with immobilized $\text{Fe}(\text{envC})_3$. The chip was exposed to compounds for 60s, followed by 300s dissociation time. Data were collected from -50 to 360 s and are shown expanded in the figure between -10 to 150 s. **A.** Compound **4**, at concentrations 6.25, 3.13, 1.56 μM ; **B.** Compound **11**, at concentrations 6.25, 3.13, 1.56, 0.78 μM ; **C, D.** Compound **8**, at concentrations 6.25, 3.13, 1.56, 0.78, 0.39 μM . Data were fit to a 1:1 binding kinetic model (A – C) or assuming bivalent analyte (D). Residuals between observed and calculated data are shown below each sensorgram.

low precision in k_a and the inability to reach saturating concentrations of analyte.

3.4.1 A bivalent model gave an improved fit to the SPR data for the dimers We observed improved fits to the data for the dimers using a bivalent analyte binding model provided by the Biacore software, (Figure 7D and S4D). The results of the data fitting are shown in Table 4.

The observation that $k_{d1} > k_{d2}$ suggested that bivalent interactions make an important contribution to slowing the off-rate, and therefore to potency against fusion.

	k_{a1} ($M^{-1}s^{-1}$)	k_{d1} (s^{-1})	K_{D1} (M)	k_{a2} ($RU^{-1}s^{-1}$)	k_{d2} (s^{-1})	RU_{max} (RU)	χ^2 (RU^2)
7	2691	0.0869	3.2e-5	4.54e-5	0.0145	160	2.95
8	1489	0.0638	4.3e-5	2.27e-5	0.0033	157	0.44

3.4.2 Kinetic rates correlated with inhibitor potency The relatively small change in K_I between monomers and dimers can be explained by the high entropic penalty due to constraining the flexible structures. **7** and **8** have 35 and 33 rotatable bonds, respectively, 19 of which involve the flexible succinimidyl-PEG₃ linker.⁴³ For the extended monomers, observed K_I were lower and k_a 's higher than for the dimers, confirming that the additional hydrophobic contribution to enthalpy more than offset the entropic penalty due the 18 – 19 added rotatable bonds. The biophysical properties of the dimers provided evidence that slow kinetics was a more important quality for inhibiting fusion than the K_I , since **7** and **8** were more than an order of magnitude more potent as fusion inhibitors than **3** and **4**, and several times more potent than **10** and **11**.

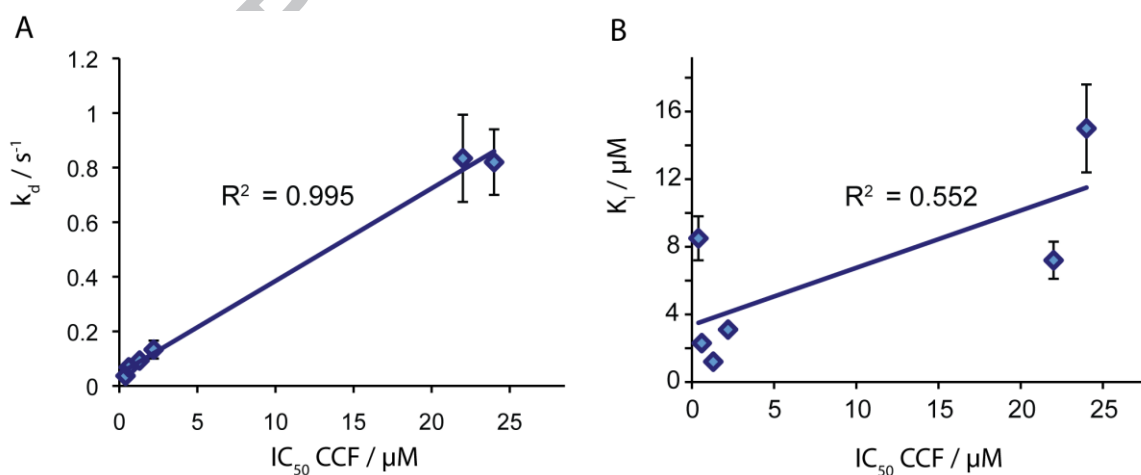


Figure 8. Correlations between kinetic data and fusion inhibition. A. Dissociation rate k_d and B. Inhibition constant K_I plotted against cell- cell fusion IC_{50} . Data were obtained from Tables 1 – 3.

They also explain the lower correlation observed between fusion inhibition and K_I compared to k_d , as shown in Figure 8. We note that k_a also correlated with inhibitor potency (not shown).

4. Discussion

In this study, we evaluated the binding affinity, kinetics and biological activity of peptidomimetic inhibitors that were modified to extend interactions with gp41 beyond the HP. The core units were arylalkoxy-amino acid helical mimetics supporting side chains at the equivalent of i and $i+3$ positions of a helix. These were **3** (H_2N -[Trp]-Trp-OH) and **4** (H_2N -[Phe4Cl]-Trp-OH). Previous studies have identified these molecules as moderate hydrophobic pocket binders and fusion inhibitors.^{23, 24} Onto these monomeric units, we grafted a largely flexible hydrophobic tail that could extend the interaction of the inhibitor into the long hydrophobic groove (compounds **10** and **11**). Alternative structures were created with a flexible PEG linker supporting two monomeric units at either end, which could purportedly interact simultaneously with hydrophobic pockets on two faces of the coiled coil. These were compounds **7** (dimer of $-HN$ -[Trp]-Trp-OH) and **8** (dimer of $-HN$ -[Phe4Cl]-Trp-OH). Fusion inhibition studies revealed that monomers were poor to moderate inhibitors, monomers extended with a hydrophobic tail were more potent, and the bivalent compounds with a monomer unit at each end of the long 22.5 Å spacer were the most potent fusion inhibitors. K_I 's were obtained by equilibrium binding studies using fluorescence, and kinetic data were obtained by SPR. Data for **3**, **4**, **10**, and **11** conformed to a 1:1 binding model, while data for the dimers **7** and **8** were commensurate with bidentate binding. Optimal fits of the dimer data were obtained with a 1:2 ligand : HP binding model (Figures 5 and 7), yielding two inhibition constants K_{I1} and K_{I2} for the first and second binding event, or by proportionate reduction in binding site concentration in a 1:1 model in which a maximum of two dimer molecules associate with each HR1 trimer,

yielding a single average $\langle K_I \rangle$. Significantly reduced dissociation constants were obtained compared to monomers, presumably due to rebinding events. The data could be interpreted as monodentate binding of dimer molecules, although this required the assumptions that 40% of the receptor aggregated during the binding assay, and that slow dissociation was simply a consequence of the large number of degrees of freedom in the dimers.⁴⁴

The variation of K_I 's across the data set was lower than the differences in their biological activity. The 6-fold reduction in K_I caused by adding a flexible hydrophobic tail in **10** and **11** improved biological activity by a factor of 10 - 15, while dimers **7** and **8** were 40 – 60 fold more active than the monomers against fusion, despite only 2 -3 fold changes to $\langle K_I \rangle$. Examination of the kinetic data revealed that dissociation rate k_d was better correlated to biological activity than K_I . Dimers dissociated ~ 20 times more slowly than monomers.

k_a also decreased with increasing size of the inhibitors, a consequence of both size and the loss of conformational entropy upon binding.⁴⁴ Consequently, the range of $K_I = k_d/k_a$ remained small. This is the enthalpy – entropy compensation effect, whereby structural mobility provided for enthalpic contributions through enhanced conformational search space and number of interactions, but simultaneously resulted in a large entropic penalty from inhibitor rigidification upon binding.⁴³ In this context, even the monomeric units with 8 - 9 rotatable bonds have poor avidity. The number of rotatable bonds increased to 18-19 for **11** and **10**, and 33 – 35 for **8** and **7**, clearly a limiting factor in the potency of the resulting molecules. It also affected the degree of cooperativity of bidentate binding in the dimers. Slight cooperativity was apparent from the lower average inhibition constant of dimers compared to monomers and the observation of $K_{I2} \ll K_{I1}$, and $k_{d2} < k_{d1}$ in bivalent model fitting, but it was significantly

dampened by the length and flexibility of the spacer between the two monomers, resulting in a large K_{I1} and low k_{a1} .

By contrast, there was significant cooperativity observed in fusion inhibitory activity of the dimers, suggesting that the biological milieu is not emulated by the biophysical setup. A factor of 2 – 3 in $\langle K_I \rangle$ became a factor of 40 – 60 in IC_{50} . One possible explanation is that the transient nature of the biological target accentuates the role of inhibitor kinetics in potency. Previous studies have shown that potency of HP binding inhibitors is highly dependent on the rate of the fusion reaction.²¹ The low off-rate for the dimers could result in gp41 molecules trapped in the inhibitor-bound state or cause an off-pathway effect.³⁹ Another possibility is that the local environment of gp41 near the membrane alters the behavior of the inhibitors due to association of hydrophobic moieties with lipids. Addition of a lipid-binding moiety to a peptide is known to enhance peptide potency by orienting and concentrating the peptide at the site of action.⁴⁵⁻⁴⁷ Yet a third possible explanation is that the cooperativity does not arise from bidentate interactions with one HR1 trimer, but rather by the bridging of two trimers on the cell or virion surface. This was suggested to be the mechanism of 20 – 100 fold increased potency of bivalent sialosides against Influenza Virus mediated hemagglutination, where, similar to our observations, a minimal increase in binding affinity to an isolated trimer occurred for the dimers.⁴⁸ This mechanism appears somewhat less likely due to the low receptor density on the surface of HIV, where there are estimated to be ~ 14 Env trimers per virion, compared to ordered arrays of 500 – 1000 HA trimers per Influenza virion.^{48,49} However, if more than one HIV Env trimer congregates to form the fusion pore, it could provide a window of susceptibility for a dimer bridge. The number is not known and has been variously thought to be one or a few.⁵⁰

5. Conclusion

In conclusion, we have observed ~ 50 fold improvement in fusion inhibitory activity upon dimerization of small peptidomimetic two-subunit compounds containing Trp and Phe4Cl residues. Off-rate was found to be a more sensitive predictor of fusion inhibitory activity than K_I . Our data are consistent with bidentate binding of the dimer molecules to the gp41 trimer, with slow dissociation rates due to rebinding events, notwithstanding the low cooperativity of dimer binding. The failure of solution binding to recapitulate the cooperative effect observed in fusion inhibition is likely due to linker flexibility and to the effect of kinetics on the inhibitory potency of the dimers. By way of comparison, a range of 10 - 300 fold improvement in fusion inhibitory activity was found by dimerizing D-peptide inhibitors, a variation that was related to the viral strain-dependent rate of fusion.^{20, 21} Trimerization of D-peptides improved activity by a factor of 1000 or more.^{20, 21} The mechanism was assumed to be due to tridentate binding to one HR1 trimer, but no specific experiments confirmed this binding mechanism. We have shown that multimerization is an applicable strategy for improving non-peptide fusion inhibitors. Local modifications to the structures to improve their thermodynamic parameters, as well as globally increasing multivalency, could yield orders of magnitude increase in potency. Importantly, these inhibitors utilize specific HP interactions rather than non-specific hydrophobic or electrostatic interactions⁵¹ which can yield low μM binding to gp41 HR1 but are difficult to optimize. In this regard, it is likely that non-specific hydrophobic interactions will limit our ability to optimize inhibitors such as **10** and **11**. Our results demonstrate proof of principle of a method to enhance avidity of non-peptide fusion inhibitors by focusing on multiple HP interactions.

Acknowledgement

This work was supported by NIH grants GM087998 and AI122847 to MG and internal funds from Touro University California and Southern Research Institute. Molecular graphics images were produced using the UCSF Chimera package from the Resource for Biocomputing, Visualization, and Informatics at the University of California, San Francisco (supported by NIH P41 RR-01081). The authors are grateful to OpenEye Scientific Software for the academic license.

ACCEPTED MANUSCRIPT

References

1. Chan, D. C.; Chutkowski, C. T.; Kim, P. S. *Proc. Natl. Acad. Sci. USA* **1998**, *95*, 15613.
2. Buzon, V.; Natrajan, G.; Schibli, D.; Campelo, F.; Kozlov, M. M.; Weissenhorn, W. *PLoS Pathog* **2010**, *6*, e1000880.
3. Weissenhorn, W.; Dessen, A.; Calder, L. J.; Harrison, S. C.; Skehel, J. J.; Wiley, D. C. *Mol. Membr. Biol.* **1999**, *16*, 3.
4. Gallo, S. A.; Finnegan, C. M.; Viard, M.; Raviv, Y.; Dimitrov, A.; Rawat, S. S.; Puri, A.; Durell, S.; Blumenthal, R. *Biochim. Biophys. Acta* **2003**, *1614*, 36.
5. Zhou, G.; Sofiyev, V.; Kaur, H.; Snyder, B. A.; Mankowski, M. K.; Hogan, P. A.; Ptak, R. G.; Gochin, M. *J. Med. Chem.* **2014**, *57*, 5270.
6. Zhou, G.; Wu, D.; Snyder, B.; Ptak, R. G.; Kaur, H.; Gochin, M. *J. Med. Chem.* **2011**, *54*, 7220.
7. Liu, S.; Wu, S.; Jiang, S. *Curr. Pharm. Des.* **2007**, *13*, 143.
8. Wang, Y.; Lu, H.; Zhu, Q.; Jiang, S.; Liao, Y. *Bioorg. Med. Chem. Lett.* **2010**, *20*, 189.
9. Naider, F.; Anglister, J. *Curr. Opin. Struct. Biol.* **2009**, *19*, 473.
10. He, Y.; Xiao, Y.; Song, H.; Liang, Q.; Ju, D.; Chen, X.; Lu, H.; Jing, W.; Jiang, S.; Zhang, L. *J. Biol. Chem.* **2008**, *283*, 11126.
11. Matthews, T.; Salgo, M.; Greenberg, M.; Chung, J.; DeMasi, R.; Bolognesi, D. *Nat Rev Drug Discov* **2004**, *3*, 215.
12. Smith, J. A.; Amagasu, S. M.; Hembrador, J.; Axt, S.; Chang, R.; Church, T.; Gee, C.; Jacobsen, J. R.; Jenkins, T.; Kaufman, E.; Mai, N.; Vickery, R. G. *Mol. Pharmacol.* **2006**, *69*, 921.
13. Choi, S.-K. *Synthetic Multivalent Molecules: Concepts and Biomedical Applications*: John Wiley & Sons, 2004.
14. Cai, L.; Gochin, M. *Antimicrob. Agents Chemother.* **2007**, *51*, 2388.
15. Cole, J. L.; Garsky, V. M. *Biochemistry (Mosc.)* **2001**, *40*, 5633.
16. Oishi, S.; Ito, S.; Nishikawa, H.; Watanabe, K.; Tanaka, M.; Ohno, H.; Izumi, K.; Sakagami, Y.; Kodama, E.; Matsuoka, M.; Fujii, N. *J. Med. Chem.* **2008**, *51*, 388.
17. Liu, S.; Jing, W.; Cheung, B.; Lu, H.; Sun, J.; Yan, X.; Niu, J.; Farmar, J.; Wu, S.; Jiang, S. *J. Biol. Chem.* **2007**, *282*, 9612.
18. Ling, Y.; Xue, H.; Jiang, X.; Cai, L.; Liu, K. *Bioorg. Med. Chem. Lett.* **2013**, *23*, 4770.
19. Eckert, D. M.; Malashkevich, V. N.; Hong, L. H.; Carr, P. A.; Kim, P. S. *Cell* **1999**, *99*, 103.
20. Welch, B. D.; VanDemark, A. P.; Heroux, A.; Hill, C. P.; Kay, M. S. *Proc. Natl. Acad. Sci. U. S. A.* **2007**, *104*, 16828.
21. Welch, B. D.; Francis, J. N.; Redman, J. S.; Paul, S.; Weinstock, M. T.; Reeves, J. D.; Lie, Y. S.; Whitby, F. G.; Eckert, D. M.; Hill, C. P.; Root, M. J.; Kay, M. S. *J. Virol.* **2010**, *84*, 11235.
22. Shaginian, A.; Whitby, L. R.; Hong, S.; Hwang, I.; Farooqi, B.; Searcey, M.; Chen, J.; Vogt, P. K.; Boger, D. L. *J. Am. Chem. Soc.* **2009**, *131*, 5564.
23. Whitby, L. R.; Boyle, K. E.; Cai, L.; Yu, X.; Gochin, M.; Boger, D. L. *Bioorg. Med. Chem. Lett.* **2012**, *22*, 2861.
24. Gochin, M.; Whitby, L. R.; Phillips, A. H.; Boger, D. L. *J. Comput. Aided Mol. Des.* **2013**, *27*, 569.
25. Gochin, M. *Assay Drug Dev Technol* **2012**, *10*, 407.

26. Derdeyn, C. A.; Decker, J. M.; Sfakianos, J. N.; Wu, X.; O'Brien, W. A.; Ratner, L.; Kappes, J. C.; Shaw, G. M.; Hunter, E. *J. Virol.* **2000**, *74*, 8358.
27. Wei, X.; Decker, J. M.; Liu, H.; Zhang, Z.; Arani, R. B.; Kilby, J. M.; Saag, M. S.; Wu, X.; Shaw, G. M.; Kappes, J. C. *Antimicrob. Agents Chemother.* **2002**, *46*, 1896.
28. Ciminale, V.; Felber, B. K.; Campbell, M.; Pavlakakis, G. N. *AIDS Res. Hum. Retroviruses* **1990**, *6*, 1281.
29. Lackman-Smith, C.; Osterling, C.; Luckenbaugh, K.; Mankowski, M.; Snyder, B.; Lewis, G.; Paull, J.; Profy, A.; Ptak, R. G.; Buckheit, R. W., Jr.; Watson, K. M.; Cummins, J. E., Jr.; Sanders-Beer, B. E. *Antimicrob. Agents Chemother.* **2008**, *52*, 1768.
30. Kagiampakis, I.; Gharibi, A.; Mankowski, M. K.; Snyder, B. A.; Ptak, R. G.; Alatas, K.; LiWang, P. J. *Antimicrob. Agents Chemother.* **2011**, *55*, 264.
31. Popovic, M.; Read-Connole, E.; Gallo, R. C. *Lancet* **1984**, *2*, 1472.
32. Popovic, M., S. ; Gartner, E.; Read-Connole, B.; Beaver, M.; Reitz, M. In *Retroviruses of human AIDS and related animal diseases.*; Valette, L., Girard, M., Eds.; Pasteur Vaccins: Marnes-La-Coquette, France., 1989, pp. 219.
33. Chackerian, B.; Long, E. M.; Luciw, P. A.; Overbaugh, J. J. *J. Virol.* **1997**, *71*, 3932.
34. Ratner, L.; Haseltine, W.; Patarca, R.; Livak, K. J.; Starcich, B.; Josephs, S. F.; Doran, E. R.; Rafalski, J. A.; Whitehorn, E. A.; Baumeister, K.; et al. *Nature* **1985**, *313*, 277.
35. Hawkins, P. C.; Nicholls, A. *J Chem Inf Model* **2012**, *52*, 2919.
36. Hawkins, P. C.; Skillman, A. G.; Warren, G. L.; Ellingson, B. A.; Stahl, M. T. *J Chem Inf Model* **2010**, *50*, 572.
37. Gochin, M.; Zhou, G. *Curr Topics Med Chem* **2011**, *11*, 3022.
38. Steger, H. K.; Root, M. J. *J. Biol. Chem.* **2006**, *281*, 25813.
39. Kahle, K. M.; Steger, H. K.; Root, M. J. *PLoS Pathog* **2009**, *5*, e1000674.
40. Hou, Y.; Gochin, M. *Anal. Chem.* **2008**.
41. Muller, K. M.; Arndt, K. M.; Pluckthun, A. *Anal. Biochem.* **1998**, *261*, 149.
42. Quinn, J. G.; O'Neill, S.; Doyle, A.; McAtamney, C.; Diamond, D.; MacCraith, B. D.; O'Kennedy, R. *Anal. Biochem.* **2000**, *281*, 135.
43. Ferrante, A.; Gorski, J. *J. Mol. Biol.* **2012**, *417*, 454.
44. Pan, A. C.; Borhani, D. W.; Dror, R. O.; Shaw, D. E. *Drug Discov Today* **2013**, *18*, 667.
45. Wexler-Cohen, Y.; Shai, Y. *PLoS Pathog* **2009**, *5*, e1000509.
46. Wexler-Cohen, Y.; Shai, Y. *FASEB J.* **2007**, *21*, 3677.
47. Ingallinella, P.; Bianchi, E.; Ladwa, N. A.; Wang, Y. J.; Hrin, R.; Veneziano, M.; Bonelli, F.; Ketas, T. J.; Moore, J. P.; Miller, M. D.; Pessi, A. *Proc. Natl. Acad. Sci. U. S. A.* **2009**, *106*, 5801.
48. Glick, G. D.; Toogood, P. L.; Wiley, D. C.; Skehel, J. J.; Knowles, J. R. *J. Biol. Chem.* **1991**, *266*, 23660.
49. Schiller, J.; Chackerian, B. *PLoS Pathog* **2014**, *10*, e1004254.
50. Wilen, C. B.; Tilton, J. C.; Doms, R. W. *Cold Spring Harb Perspect Med* **2012**, *2*.
51. Gochin, M.; Cai, L. *J. Med. Chem.* **2009**, *52*, 4338.

Figure Captions

Figure 1. Experimental and model structures of the gp41 HR1 – HR2 domain and interactions.

A. Homology modeling of HIV-1 HXB2 ectodomain from the structure of the corresponding SIV domain (pdb 2EZO). The HR1 trimer is shown as a space filling model in tan, and loop and HR2 residues are shown as a ribbon representation in yellow; B. Expansion of the hydrophobic pocket region from A. C. Crystal structure (pdb 2R5D) of D-peptide PIE7 showing Trp and Leu residues filling the pocket; D, E. Modeled low energy structures of two subunit and three subunit peptidomimetics with Trp and Leu residues filling the pocket. See Figure 2 for the structures of the peptidomimetic inhibitors.

Figure 2. Structures of peptidomimetic inhibitors used in this study.

Figure 3. Model showing the ability of dimer **7** to reach around the HR1 coiled coil with the terminal –NH-[Trp]-Trp-OH units interacting in two hydrophobic pockets. The surface representation of the HR1 (pdb 3P7K) has been made partly transparent to reveal the docked aromatic rings of **7**.

Figure 4. Dose-response curves for each compound demonstrating percent inhibition of cell-cell fusion (A, B) and Ba-L viral infectivity (C, D) measured as relative luminescence units (RLU) using a luciferase reporter. A, C. Compounds **3** (blue), **7** (black), **10** (red); B, D. Compounds **4** (blue), **8** (black) and **11** (red). Cell viability is shown in corresponding open circles. Error bars are standard deviations of three measurements.

Figure 5. Fluorescence competitive inhibition dose response curves performed with 7.2 μ M binding sites. A. **3** (blue), **7** (black), **10** (red) and B. **4** (blue), **8** (black), **11** (red). C and D show data fitting for dimers **7** and **8** to a 1:1 binding model (dashed line) and 1:2 binding model (bold solid line) assuming 7.2 μ M binding sites. The narrow solid lines show an alternative fit to a 1:1

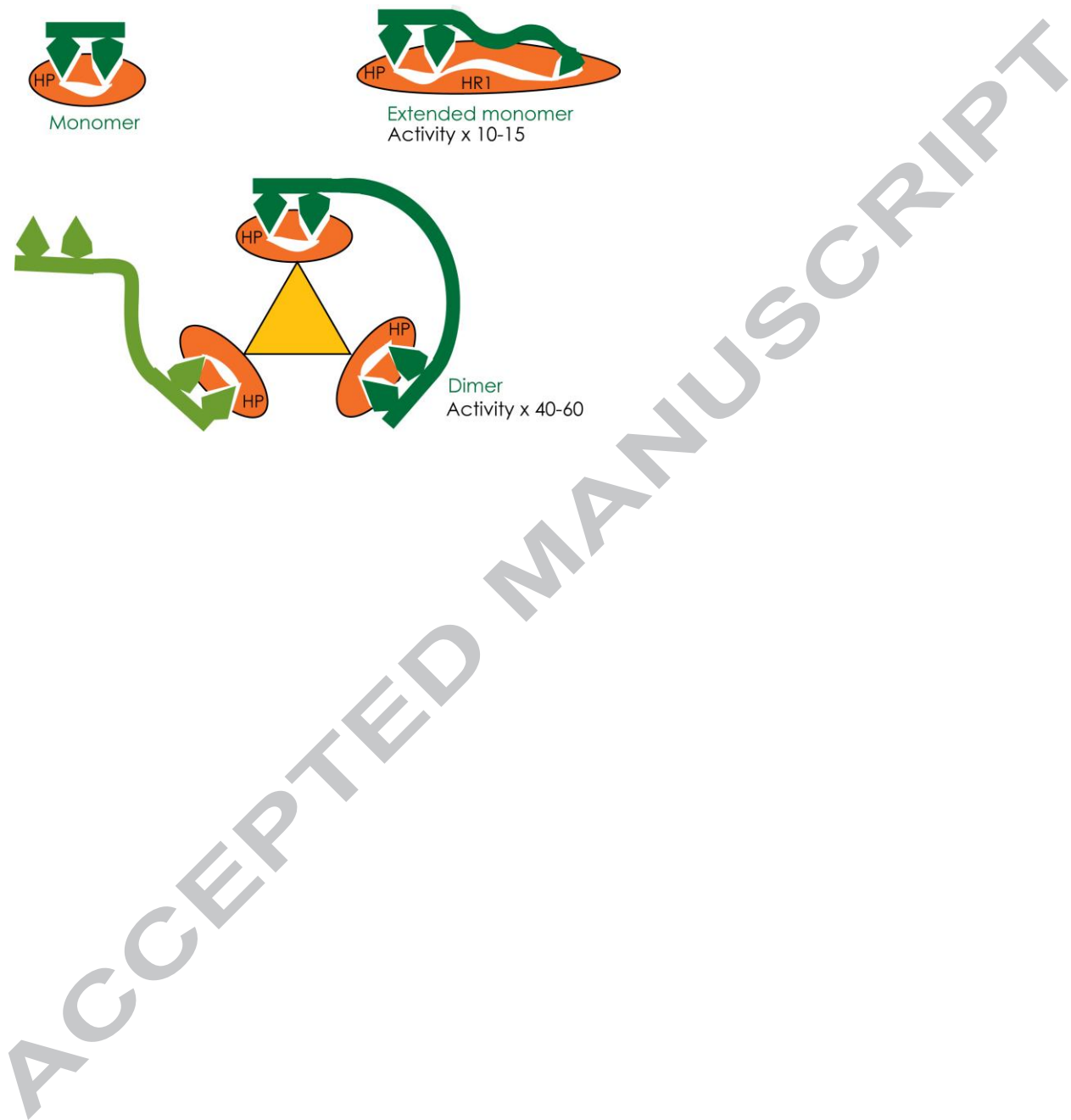
binding model with 40% reduced receptor concentration. RFU = relative fluorescence units, as a fraction of the fluorescence of probe plus compound in the absence of receptor (F_L).

Figure 6. A model of bidentate binding of dimers to the HR1 trimer. The HP's, shown in orange, are arranged on a three-fold axis of symmetry. Each green diamond shape represents an aromatic side chain of the 2-subunit peptidomimetic monomer. Two equivalent dimers are depicted in green and light green.

Figure 7. SPR sensorgrams obtained with immobilized $\text{Fe}(\text{envC})_3$. The chip was exposed to compounds for 60s, followed by 300s dissociation time. Data were collected from -50 to 360 s and are shown expanded in the figure between -10 to 150 s. **A.** Compound **4**, at concentrations 6.25, 3.13, 1.56 μM ; **B.** Compound **11**, at concentrations 6.25, 3.13, 1.56, 0.78 μM ; **C, D.** Compound **8**, at concentrations 6.25, 3.13, 1.56, 0.78, 0.39 μM . Data were fit to a 1:1 binding kinetic model (A – C) or assuming bivalent analyte (D). Residuals between observed and calculated data are shown below each sensorgram.

Figure 8. Correlations between kinetic data and fusion inhibition. A. Dissociation rate k_d and B. Inhibition constant K_I plotted against cell- cell fusion IC_{50} . Data were obtained from Tables 1 – 3.

Graphical Abstract



Highlights

- Bivalent gp41 inhibitors were 40 – 60 fold more potent than monomers.
- Binding potency was not significantly improved by dimerization.
- Potency was correlated to slower off-rates.
- Data could be explained by a bidentate binding model for the dimers.
- The kinetic dependence may be due to transience of the targeted intermediate.

ACCEPTED MANUSCRIPT